Structurally distinct endocytic pathways for B cell receptors in B lymphocytes

Thaddeus M. Davenport, Andrea M. Dickey, Regina Ahn, Aleah D. Roberts, Kem A. Sochacki, Justin W. Taraska*

Laboratory of Molecular Biophysics, 50 South Drive, Building 50, National Heart, Lung, and Blood Institute, National Institutes of Health, Bethesda, MD 20892

*Corresponding author: justin.taraska@nih.gov

Key words. Endocytosis, B Cell, Antigen, Clustering, Nano-scale, CLEM, B Cell Receptor, Lymphocyte, Super-resolution, Electron Microscopy, Correlative Microscopy.

ABSTRACT

B lymphocytes play a critical role in adaptive immunity. Upon antigen binding, B cell receptors (BCR) cluster on the plasma membrane and are internalized by endocytosis. B cells capture diverse antigens in various contexts and concentrations. However, it is unclear whether the mechanism of BCR endocytosis changes in response to these factors. Here, we studied the concentration dependence of anti-human IgM Fab'2-induced BCR clustering and internalization in the human IgM+ DG-75 B cell line using advanced imaging methods, including correlative super resolution fluorescence and electron microscopy. By directly visualizing nanoscale structures associated with BCR clusters, we provide evidence that BCR cluster size increases with Fab'2 concentration and the mechanism of internalization switches in response to BCR cluster size. At low concentrations of Fab'2, B cells internalize BCR clusters by classical clathrin-mediated endocytosis. However, at high Fab'2 concentrations, B cells retrieve clathrin-bound BCR clusters using large invaginations of the plasma membrane.

INTRODUCTION

B lymphocytes are critical in adaptive immune responses to pathogens (Trombetta and Mellman, 2005). Dysregulation of B cell activity can lead to cancer, autoimmunity, and allergy (Avalos et al., 2014). The B cell receptor (BCR), abundant in the plasma membrane of B cells, binds to and internalizes antigens for processing and presentation to T cells (Clark et al., 2004; Harwood and Batista, 2010). BCR activation, along with T cell engagement, promotes the expansion of a clonal lineage of antigen-specific B cells. As a first step in this process, clustering of BCRs in response to antigen binding initiates a signaling cascade that triggers the rapid internalization of receptor/antigen complexes (Harwood and Batista, 2010; Pierce and Liu, 2010). Antigen structure, concentration, and presentation may all influence the size of BCR/antigen clusters formed on the plasma membrane (Batista et al., 2001; Srinivas Reddy et al., 2011; Thyagarajan et al., 2003). The radii of these clusters can vary from ~60 nm to over 1 micron (Lee et al., 2017; Pierce and Liu, 2010; Stone et al., 2017). The cellular pathways that enable B cells to specifically internalize antigen in spite of such structural variability are unclear.

Clathrin-mediated endocytosis (CME) is the primary mechanism of endocytosis in eukaryotic cells (Conner and Schmid, 2003; McMahon and Boucrot, 2011; Mettlen et al., 2018). In CME, adaptors,

accessory proteins, and cargo recruit clathrin to the inner leaflet of the plasma membrane where it assembles as a curving lattice that drives the formation of cargo-filled membrane vesicles (McMahon and Boucrot, 2011; Mettlen et al., 2018). Clathrin has been shown to play an important role in BCR endocytosis and BCR signaling (Natkanski et al., 2013; Salisbury et al., 1980; Stoddart et al., 2005). For example, knockdown of clathrin dramatically impairs BCR internalization (Stoddart et al., 2005). In addition, mutation of clathrin-adaptor domains found in the BCR complex results in constitutively active receptors that accumulate at the plasma membrane and are observed in lymphomas (Davis et al., 2010). The precise role of clathrin in BCR endocytosis, however, is not well defined.

While clathrin has been shown to be important for BCR endocytosis, B cells can still retrieve BCRs in the absence of clathrin (Stoddart et al., 2005). This raises the possibility that there may be other mechanisms of BCR internalization. A number of alternative uptake pathways have been described in eukaryotic cells (Mayor et al., 2014; Watanabe and Boucrot, 2017). These clathrin-independent endocytosis (CIE) pathways include micron-scale pinocytosis and phagocytosis, as well as nanometer-scale mechanisms such as caveolae, flotillin-based, endophilin-based, actin-based, and other less well-defined vesicle processes (Ferreira and Boucrot, 2018; Mayor et al., 2014). Thus, it is not known if CIE uptake pathways exist for B cell receptors or if a unique hybrid form of endocytosis operates during antigen-mediated BCR internalization. In support of the latter, previous work has shown that B cells are capable of internalizing large cargo through a process akin to phagocytosis (Souwer et al., 2009). Though not all cargos are oversized, this capacity for phagocytic-like processes is consistent with observations that actin and myosin play a particularly important role in antigen-mediated BCR clustering, activation, and internalization (Brown and Song, 2001; Tolar, 2017). Furthermore, large pieces of B cell and target membrane are internalized when B cells interact with antigen presented on membranes (Natkanski et al., 2013). This membrane capture process depends on clathrin, but doesn't appear to wholly resemble classic clathrin-mediated endocytosis in size, structure, or molecular composition (Natkanski et al., 2013).

How antigen concentration impacts the structure or mechanism of BCR endocytosis is also unclear. Concentration-dependent internalization mechanisms have been proposed for many receptors such as epidermal growth factor receptor (EGFR)(Tomas et al., 2014). Low concentrations of epidermal growth factor (EGF) stimulate EGFR uptake by a clathrin-dependent mechanism, but at high EGF concentrations internalization occurs by a mixture of clathrin-dependent and clathrin–independent mechanisms (Sigismund et al., 2008). Such behavior has not been described for BCR. However, B cells might benefit from such a concentration-dependent switch in the mechanism of BCR endocytosis. By adjusting the endocytic mechanism of BCR uptake in response to antigen concentrations, B cells might be better able to rapidly and appropriately responded to a wide-range of changes in the concentration of foreign antigens during infection. Likewise, B cells could avoid inappropriate or unnecessary responses to ubiquitous self-antigens or transient exposures to foreign molecules. However, no systematic study has been made to directly visualize the nanoscale structural changes in the plasma membrane of B cells during antigen challenge.

Here, we study anti-human IgM Fab'2-induced endocytic structures in the DG-75 human B cell line to understand the mechanism of BCR internalization. First we measure BCR internalization in live cells and observe the dynamics of antigen-induced BCR clustering and internalization in real time with flow cytometry and live cell imaging. Next, we map the molecular components of early BCR endocytic structures with total internal reflection fluorescence microscopy. Finally, we use correlative super resolution fluorescence and platinum replica transmission electron microscopy (CLEM) to directly examine the nanoscale architecture of BCR endocytic structures following antigen stimulation across a range of activating ligand concentrations and times. We show that BCR clusters induced by increasing concentrations of Fab'2 and time are captured by distinct nanoscale endocytic structures. This work provides direct structural evidence for the complexity of BCR endocytosis and provides insights into a mechanism of endocytosis that allows B cells to tailor their endocytic machinery to accommodate a wide variety of antigen-induced BCR cluster sizes.

RESULTS

First, to characterize the temporal and spatial dynamics of BCR internalization in our system, we imaged live DG-75 cells with confocal microscopy (Figure 1a-b). Cross-linking anti-human IgM Fab'2 antibody was added to DG-75 cells to a final concentration of 12 µg/mL at 37°C to induce activation and internalization of native BCRs labeled with fluorescent Fab fragments. Five minutes after the addition of the bivalent Fab'2 ligand, cell-surface BCRs formed small patches that condensed into larger clusters and were internalized into the cytoplasm over a period of 30 minutes (Figure 1a-b). In some cases, less uptake was observed, and receptors were retained on the surface in large BCR cluster "caps" (Supplementary figure 1). These results are supported by thin section transmission electron microscope (TEM) images of B cells stimulated in the presence of membrane-bound ferritin, a small electron-dense indicator that labels the outer leaflet of the plasma membrane and inner leaflet of endocytic vesicles. In unstimulated cells little internalization of ferritin was observed by thin section TEM (Supplementary figure 2), but large ferritin-positive endocytic structures were observed attached to the plasma membrane and deeper in the cytosol after cells were stimulated for 15 minutes with 8 µg/mL anti-human IgM Fab'2 (Supplementary figure 3).

To better understand the kinetics and concentration-dependence of BCR internalization at a population level, we developed a flow cytometry-based internalization assay. Specifically DG-75 cells were co-stained with two anti-IgM Fabs conjugated to either a pH-sensitive FITC fluorophore or a pH-insensitive Alexa Fluor 647 fluorophore. By measuring changes in both FITC and Alexa Fluor 647 fluorescence following Fab'2 stimulation, we could distinguish between signal decreases due to acidification of internalized Fab-labeled BCR in endocytic vesicles and a loss of fluorescence due to Fab dissociation from the plasma membrane. Changes in Alexa Fluor 647 fluorescence were small compared to those of FITC fluorescence, indicating that internalization into low pH vesicles rather than dissociation from the membrane was the major source of the observed changes in mean fluorescence intensity (MFI) (Figure 1c). Using this assay to monitor BCR uptake, we tested the dependence of BCR internalization on the concentration of Fab'2 by stimulating DG-75 cells with Fab'2 at concentrations ranging from 0-14 µg/mL. The overall rate of internalization did not vary dramatically with Fab'2 concentration, as the time to half-

maximal internalization was ~15 minutes for all concentrations tested (Figure 1d). However, the amount of measured BCR internalization at the final time point did vary in a concentration-dependent manner, with the most BCR internalization observed at 3.5 µg/mL Fab'2 (Figure 1e). No additional change in signal occurred at higher concentrations of Fab'2. In spite of the variability, the rate of BCR internalization observed by live cell microcopy matched the flow cytometry data and together indicate that antibody-induced BCR uptake in DG-75 cells occurs over a period of 30 minutes, with similarly efficient internalization of BCR exposed to concentrations of Fab'2 above 1.75 µg/mL. Thus, B cells can accommodate the uptake of BCRs across a wide range of cross-linking antigen concentrations.

Because clathrin has been previously shown to be involved in BCR internalization, we next tested whether clathrin colocalizes with BCR clusters in stimulated DG-75 cells (Natkanski et al., 2013; Salisbury et al., 1980). B cells, labeled with anti-IgM Fab-Alexa Fluor 594, were stimulated with Fab'2 at 37°C and diluted into cold imaging buffer to halt internalization while the cells settled onto coverslips prior to chemical fixation, permeabilization, and immunolabeling for clathrin. Equatorial slices of cells show that, as in the live-cell experiments, BCR spots form on the plasma membrane after 5 min of stimulation. At these plasma membrane BCR structures, we observed colocalization with clathrin after stimulating with low (2 µg/ml) and a relatively high (8 µg/mL) concentration of Fab'2 (Figure 1f). This is consistent with previous studies that clathrin is involved in the internalization of BCRs (Natkanski et al., 2013; Stoddart et al., 2005).

Using total internal reflection fluorescence microscopy (TIRF), we further examined whether other classic endocytic proteins colocalize with BCR clusters on the plasma membrane (Larson et al., 2014). We imaged DG-75 cells co-transfected with IgM-GFP and several clathrin-associated proteins tagged with mCherry to measure colocalization following stimulation with 12 µg/mL Fab'2. After 5 min at 37°C, BCR clusters showed colocalization with endocytic proteins including AP2, Eps15, FCHO1, clathrin, CALM, Epsin1, HIP1R, and Dynamin-2 (Figure 1g). The correlation values between BCRs and dynamin were slightly lower than those of the other proteins, possibly reflecting the early stage of BCR clustering and the late-stage role of dynamin in the scission of the clathrin-coated vesicles from the plasma membrane (Taylor et al., 2011). Interestingly, BCR clusters did not show substantial colocalization with the transferrin receptor (Tfr) (Figure 1g), a classical cargo of clathrin-mediated endocytosis (Harding et al., 1983; Taylor et al., 2011). This suggests that clathrin structures associated with Fab'2-induced BCR clusters may be distinct from the pool of clathrin-coated structures that internalize transferrin receptor, though BCR may later traffic through endosomal compartments containing Tfr. Likewise, little actin was observed associated with BCR clusters in the plane of the plasma membrane by TIRF. Although actin was not concentrated on BCR clusters within 100 nm of the plasma membrane, we cannot rule out that it may associate with the periphery or very top of deeply-invaginated BCR structures, as suggested by previous work (Onabajo et al., 2008). These data indicate that many classical CME-associated proteins assemble with BCR clusters at the plasma membrane during receptor activation.

To determine whether the concentration of Fab'2 alters the nanoscale structure and distribution of BCRs in the B cell plasma membrane, we measured the size of BCR clusters using direct stochastic optical reconstruction microscopy (dSTORM), a super-resolution localization microcopy method (Figure

2)(Betzig et al., 2006; Heilemann et al., 2008). Figure 2a shows representative dSTORM images of DG-75 cells stained with Alexa 647-labeled anti-human IgM Fab fragments under three conditions: unstimulated, incubated with low (2 µg/mL) or high (8 µg/mL) concentrations of Fab'2 for 15 minutes at 37°C before attachment to coverslips and fixation. In unstimulated cells, BCR fluorescence was uniformly distributed across the plasma membrane with few clusters (Figure 2a left). After 15 minutes of stimulation with 2 µg/mL Fab'2, both the distribution of BCR on the plasma membrane and the size of BCR fluorescent spots became more heterogeneous (Figure 2a center). However, the most dramatic change in BCR distribution was observed after 15 minutes of stimulation with 8 µg/mL Fab'2, which showed large clusters of BCR Fluorescence (Figure 2a right). To quantify these changes in BCR distribution, we divided BCR punctae into three groups based on their areas relative to clathrin coated pits. Clathrin pits have an area of ~ 18,000 nm^2 on average, but range from ~10,000 nm^2 to 50,000 nm^2 in area, or 55 to 125 nm in radius (Dambournet et al., 2018; Sochacki et al., 2017; Sochacki et al., 2012). In this way we defined: 1) small spots (<9600 nm^2), which are smaller than a typical clathrin coated pit; 2) intermediate spots (9600-48000 nm^2), which are comparable in size to the majority of clathrin coated pits; and 3) large fluorescent spots (>48000 nm^2), which are over 2.5 times the mean area of clathrin coated pits. Approximately 80% of the fluorescent area in unstimulated cells was composed of small punctae, with the remaining made up of spots between 9600-48000 nm^2 (Figure 2b). Large clusters made up an insignificant portion of the fluorescence in unstimulated cells. In contrast, for cells treated with 8 µg/mL Fab'2, large fluorescent punctae made up an increasing proportion of the fluorescent area – 40% and 60% - at the 5 and 15 minute time points, respectively (Figure 2b). This was not the case for cells treated with 2 µg/mL Fab'2, in which 60% of the fluorescent area was made up of small spots, although there was a slightly increased proportion of intermediate and large fluorescent clusters relative to unstimulated cells (Figure 2b). Thus, increasing the concentration of Fab'2 shifted the fluorescence of BCR to larger clusters, and after 15 minutes of stimulation with 8 µg/mL Fab'2 we predominantly observed very large BCR clusters that exceeded the membrane area of typical clathrin coated pits.

Correlative light and electron microscopy (CLEM) provides a comprehensive nanoscale structural context for proteins identified by fluorescence microscopy (Kopek et al., 2017; Sochacki et al., 2014). Figure 3 shows CLEM images of the cytoplasmic surface of an unstimulated DG-75 B cell plasma membrane. Similar to the data shown in Figure2, BCR fluorescence in unstimulated cells was characterized by small localizations, distributed randomly across the plasma membrane (Figure 3a). Figure 3b shows the corresponding platinum replica EM image of the same cell and the correlated fluorescence and EM image is shown in Figure 3c. In EM the structure of membrane adjacent actin and membrane-associated vesicles are clearly visible. With higher magnification, no obvious association of the receptor with cytoskeletal filaments or vesicles was observed (Figure 3d). Of note, cells attached to the glass generally exhibited a macroscopic ring pattern of membrane-associated actin. Figure 4 shows CLEM images of DG-75 cells after 5 minutes of stimulation with either 2 µg/mL Fab'2 (Figure 4a-d) or 8 µg/mL Fab'2 (Figure 4e-h). Unlike cells treated with 2 µg/mL Fab'2 (Figure 4d), after 5 minutes of stimulation with 8 µg/mL Fab'2, BCR clusters began to form, and these clusters were often associated with honeycomb clathrin lattices in the correlated TEM image (Figure 4h). Figure 5 shows that after 15 minutes of stimulation with 8 µg/mL Fab'2, BCR clusters were larger and were frequently correlated with dense honeycomb

arrays that were often associated with distinctive smooth, raised regions of the plasma membrane (Figure 5e-h). In contrast, cells treated with 2 µg/mL Fab'2 showed much smaller BCR fluorescence punctae and few morphological changes on the plasma membrane after 15 minutes (Figure 5a-d).

To quantitatively measure changes in membrane and organelle structures following Fab'2 stimulation, we analyzed regions of the plasma membrane in platinum replica TEM images alone (Fig 6). TEM Images were segmented for two objects: 1) Honey-comb clathrin lattices ("Clathrin") and 2) smooth, raised pieces of the plasma membrane ("Smooth Raised Membrane", SRM) (Figure 6b-e). These structures occasionally colocalized as SRMs coated with clathrin (Figure 6e). This analysis shows that the density of all clathrin-coated structures (CCS) is very low in unstimulated DG-75 cells (0.29 CCS/μm^2 +/- 0.08 SEM) relative to other mammalian cell types (Figure 6f). For example, PC12 cells have ~1.6 CCS/μm^2 and Hela cells have ~0.7 CCS/μm^2. Treatment with 8 µg/mL Fab'2 dramatically increased the amount of clathrin on the plasma membrane: at the 5 minute time point we measured 1.38 CCS/μm^2 +/- 0.48 SEM, and 1.59 CCS/μm^2 +/- 0.29 SEM after 15 minutes. There was less recruitment of clathrin to the plasma membrane following treatment with 2 µg/mL Fab'2: at 5 minutes we measured a density of 0.64 CCS/μm^2 +/- 0.11 SEM that only mildly increased at 15 minutes (0.79 CCS/μm^2 +/- 0.15 SEM) (Figure 6f). Of note, individual clathrin structures did not change in size, with the average diameter of clathrin structures remaining constant during stimulation (Figure 6g). But individual spots did cluster together, showing a closer nearest-neighbor distance than would be expected from the increased density of clathrin observed over the course of activation (Figure 6h). Figure 6i shows that the density of SRMs also increased during stimulation with the largest increase in SRMs seen after 15 minutes in cells exposed to 8 µg/mL of Fab'2. Like clathrin, these structures did not change in overall diameter (Figure 6j) and yet unlike clathrin, showed only moderate clustering (Figure 6k). Figure 6l shows that in many cases, clathrin coated structures are associated with SRM. The most dramatic association of clathrin with SRMs was observed in cells treated for 15 minutes with 8 µg/mL Fab'2. In these cells nearly all clathrin-coated structures are clustered and associated with SRMs (Figure 6l). Thus, high concentrations of Fab'2 induce the formation of large, smooth, clathrin-decorated invaginations of the plasma membrane.

The above analysis was performed only on TEM images to understand the impact of antigen activation on the structure of the plasma membrane. Next, we quantified changes in the distribution of BCR fluorescence on the plasma membrane relative to these EM-identified structures using super-resolution CLEM images. As seen in the CLEM images, BCR fluorescence did not always exclusively overlap with clathrin but was often found both on clathrin and in the area immediately surrounding clathrin structures. Thus, using the segmented objects shown in Figure 6 to identify both the directly bound and closely associated fluorescence, we measured the fraction of BCR fluorescence within a 200 nm radius of three different classified plasma membrane regions (clathrin, SRM, and clathrin located on SRMs) in the 5 different experimental conditions (Unstimulated, 5 min 2 µg/mL Fab'2, 5 min 8 µg/mL Fab'2, 15 min 2 µg/mL Fab'2, and 15 min 8 µg/mL Fab'2). Figure 7a-c shows that in unstimulated cells, few BCR fluorescent localizations were associated with clathrin, SRMs, or clathrin on SRMs. However, stimulation with 8 µg/mL Fab'2 for 5 minutes resulted in a concentration of BCR fluorescence within 200 nm of both clathrin and SRM structures, which further increased at 15 minutes. As shown in Figure 6, under these

conditions, most clathrin is found clustered on SRMs, and thus, our measurements in Figure 7 likewise show that the majority of BCR fluorescence is concentrated near these SRM-localized clathrin clusters. In contrast, cells treated with 2 µg/mL Fab'2 showed much less association of BCR fluorescence with SRM-associated clathrin. It should be noted, however, that there was little clathrin observed on SRMs under these conditions. Taken together, these data demonstrate that BCR internalization occurs with similar efficiency over a wide range of concentrations of Fab'2, but the size of BCR clusters increases with time and the structure of their associated endocytic carriers dramatically change in a Fab'2 concentration- and time dependent manner (Figure 8).

DISCUSSION

Adaptive immunity depends on the ability of B cells to capture antigen through a regulated internalization mechanism of the B cell receptor (Harwood and Batista, 2010; Hoogeboom and Tolar, 2016). Here, we provide direct structural evidence that the mechanism of BCR uptake varies with the concentration of the stimulating ligand and the size of the resulting BCR clusters (Figure 8). In unstimulated cells, we observed that BCR is distributed across the plasma membrane and the plasma membrane contains few clathrin-coated structures compared to other mammalian cell types at rest. Upon antigen stimulation, BCRs cluster in a concentration-dependent fashion and associate with a dramatically increased number of clathrin coated structures (Figure 8). At higher antigen concentrations and longer times, large clathrin-associated BCR clusters coalesce onto smooth raised membrane invaginations of the plasma membrane (Figure 8). Thus, antigen concentration impacts BCR cluster size, and cluster size is correlated with a change in the structure of the plasma membrane. Our data support a model where B cells can accommodate the internalization of a wide range of BCR cluster sizes by deploying a classic clathrin mediated endocytosis as well as a hybrid form of endocytosis that uses clathrin as a coat to cluster receptors and large membrane carriers to capture these clathrin-coated receptors wholesale into the cytoplasm (Figure 8).

Below we consider several implications of our finding on the B cell endocytic machinery. First, in unstimulated cells most BCR was not associated with clathrin. Nor were there many clathrin structures present at the membrane. Most mammalian cells maintain a dynamic population of clathrin-coated structures at the membrane at a density between 0.5 and 2 structures per square micron (Dambournet et al., 2018; Sochacki et al., 2012; Taylor et al., 2011). These structures support constitutive endocytosis and the recycling of many key receptors such as the transferrin receptor. We find that resting B cells maintain very few clathrin structures at their plasma membrane. This could serve to increase the steady-state concentration of BCRs on the surface. In contrast to unstimulated cells, nearly 100% of BCR fluorescence was associated with clathrin structures in cells treated with 8 µg/mL Fab'2 for 15 minutes. The relative absence of BCR-negative clathrin coated pits suggests that clathrin assembles specifically on antigen-induced BCR clusters. Considering the need for immune responses to be specific, regulated, and rapid, the lack of membrane-associated clathrin structures in resting B cells could serve as a barrier to limit endocytosis and minimize off-target or autoimmune responses that might occur as a result of nonspecific antigen internalization (Davis et al., 2010). Furthermore, the selective and nearly complete

recruitment of clathrin to clustered BCR would ensure specific and efficient internalization of the target antigen.

Second, clathrin-associated BCR clusters form and group together in a concentration-dependent manner following Fab'2 stimulation. Treatment with 2 µg/mL Fab'2 stimulates efficient BCR internalization by flow cytometry, and this internalization appears to involve clathrin, based on colocalization of BCR with clathrin in confocal microscopy images (Figure 1). However, CLEM data showed that this does not yield dramatic growth of BCR clusters or recruit large amounts of additional clathrin to the plasma membrane. In contrast, after 5 minutes of stimulation with 8 µg/mL Fab'2, the amount clathrin at the surface membrane increases ~5 fold, and nearly all BCR clusters are associated with clathrin. After 15 minutes of stimulation with 8 µg/mL Fab'2, BCR clusters capped with clathrin increase in number, cluster together, and are found to be largely associated with smooth, raised membrane structures (Figure 8). Thus, individual clathrin structures precede the development of SRMs capped with clathrin and BCRs. These data suggests a model in which receptor clustering and internalization compete for BCR on the plasma membrane. First, relatively small BCR clusters may be internalized through a classic clathrin-mediated endocytic pathway but BCR clusters that grow too large to be contained in a small clathrin-coated vesicle could require a hybrid mechanism of membrane internalization that involves bulk plasma membrane remodeling (Figure 8). Given the large body of literature that supports a role for lipid microdomains in BCR signaling, one avenue for future work is to examine whether the smooth, raised structures we observe by CLEM form as a result of phase transitions within the plasma membrane (Cheng et al., 1999; Sezgin et al., 2017; Stone et al., 2017).

From this model, we suggest that BCR clusters of different sizes would pose distinct challenges for the endocytic machinery and may therefore recruit distinct sets of regulatory proteins in each case. Whereas small BCR clusters may be internalized by a basic set of clathrin-associated proteins, perhaps larger BCR clusters may depend on an expanded set of endocytic proteins (Ferreira and Boucrot, 2018; Watanabe and Boucrot, 2017). For example, large BCR clusters may rely on increased involvement of actin and myosin for internalization just as very large antigens appear to do in a mechanism that more closely resembles phagocytosis (Zhu et al., 2016). Additionally, previous work has shown that B cells rely on myosin to a greater extent when internalizing antigen presented on a bilayer as compared to soluble antigen (Natkanski et al., 2013). Similar to these studies, which show context and antigen-dependent variability in the mechanism of BCR uptake, our data support the hypothesis that BCR cluster composition and size may be another factor that could impact the mechanism of BCR internalization.

We have shown that endocytic structures associated with large BCR clusters exhibit a unique nanoscale morphology. These structures exhibit dense closely-packed arrays of small clathrin structures on smooth, raised membrane invaginations. These clathrin-coated sites are unlike those observed by EM in other mammalian cell types (Dambournet et al., 2018; Scott et al., 2018; Sochacki et al., 2017; Sochacki et al., 2014). However, there is some similarity between the raised clathrin structures we observe in B cells and the structures that form on mast cells in response to FCeRI clustering (Cleyrat et al., 2013; Wilson et al., 2002). There is overlap in the BCR and FCeRI signaling cascades (Siraganian et al., 2010),

and the morphological similarity we observe in the receptors' endocytic structures suggests that there may be commonalities in their mechanisms of internalization as well.

Thus, the mechanism of BCR endocytosis may toggle according to the concentration of soluble antigen and the size of the BCR cluster. Our data support the idea that BCR endocytosis occurs by an adaptable mechanism, employing different endocytic structures to internalize BCR clusters of different sizes. It remains to be determined whether these distinct endocytic structures traffic differently throughout the cell. Future studies to understand whether these structurally distinct endocytic pathways influence the efficiency of antigen processing and presentation will be valuable to ensure that future adjuvants and immunogens are optimally designed to cooperate with the available B cell endocytic machinery.

MATERIALS AND METHODS

Cell lines and imaging reagents – The IgM+VkL+ human DG-75 B cell line was purchased from ATCC (CRL-2625) and cultured in a growth medium consisting of RPMI 1640 (-) Phenol Red with 10% FBS, 1% Penicillin/Streptomycin, 10mM HEPES pH 7.4, and 1mM Sodium Pyruvate. Cells were periodically tested for mycoplasma. Cell line identity was verified as a human B cell (ATCC). Anti-human IgM Fab and Fab'2 fragments were purchased from Jackson Immunoresearch laboratories, including: Goat Anti-Human IgM Fc5µ Fab-Fluorescein (109-097-043), Goat Anti-Human IgM Fc5µ Fab-Alexa Fluor 647 (109-607-043), Goat Anti-Human IgM Fc5µ Fab-Alexa Fluor 488 (109-547-043), Goat Anti-Human IgM Fc5µ Fab-Alexa Fluor 594 (109-587-043), and AffiniPure F(ab')2 Fragment Goat Anti-Human IgG + IgM (H+L) (109-006-127). Fixable Viability Dye eFluor450 (65-0863-18), Alexa Fluor 488 Phalloidin (A12379), mouse anti-clathrin heavy chain antibody clone X-22 (MA1065), and donkey anti-mouse Alexa Fluor647 (A31571) were purchased from ThermoFisher. Coverslips for TIRF and confocal microscopy #1.5 25mm were purchased from Warner Instruments (64-0715), and high density (400 particles /100 mm^2) wide spectral band (600+/- 100 nm) gold fiducial coverslips were purchased from Hestzig LLC. for correlative fluorescence electron microscopy. Coverslips were washed in a heated solution of hydrogen peroxide and ammonia solution as previously described (Trexler and Taraska, 2017) with gold fiducial coverslips exposed to the cleaning solution for 10 minutes. Poly-L-Lysine for coating coverslips was purchased from Sigma Aldrich (P4832).

Construction of DG-75 IgM-GFP – The DG-75 IgM VH sequence [Genbank: Z74668, (Chapman et al., 1996)] with the native VH3-23*01 leader peptide sequence [IMGT: M99660, (Matsuda et al., 1993)],was synthesized by Biobasic and cloned by overlap PCR in frame with the human IGHM sequence obtained from DNASU (HscD00445046). This fragment was then cloned by overlap PCR upstream of a PCR product encoding meGFP with an SGSGSGGSGSGGGPVAT N-terminal linker peptide. PCR reactions were carried out using Accuprime Pfx Supermix (ThermoFisher: 12344040) with primers synthesized by Integrated DNA Technologies. The DG75-VH-IgM-linker-GFP insert was digested with NheI/NotI and ligated into the Clontech pEGFP-N1 vector.

Flow cytometry-based BCR internalization assay – DG-75 cells at a concentration of 1-1.5 million cells /mL were spun down at 200xg for 5 minutes. The cell pellet was resuspended at 10 million cells/mL in a

staining medium of RPMI complete with the addition of 1:1000 anti-human IgM Fab-FITC, 1:1000 anti-human IgM-Fab-Alexa Fluor 647, and 1:1000 eFluor450 live-dead violet. Cells were stained at 4°C for 30 minutes prior to washing with RPMI complete and pelleting cells at 200xg for 5 minutes. The stained, washed cell pellet was resuspended to a concentration of 2 million cells/mL in RPMI complete, filtered through a 40-µm filter, and 700 µL of cells were aliquoted into each round bottom tube. Anti-human IgM Fab'2 was added to a final concentration of 0, 0.8, 1.7, 3.5, 7, or 14 µg/mL immediately prior to flow cytometry analysis and a temperature shift to 37°C. Cells were incubated at 37°C and analyzed every 10 minutes post-Fab'2 addition for up to 60 minutes. Gates were drawn to isolate singlet, live (eFluor450 negative) cells.

BCR internalization was measured by tracking the pH-induced decrease in FITC fluorescence that occurs as the BCR-bound FITC-conjugated Fab is internalized and trafficked into low pH endosomal compartments. To account for the change in fluorescence that may result from dissociation of fluorophore-conjugated Fab from the B cell surface over time, the change in FITC signal was corrected for the measured decrease in the fluorescence of the pH-insensitive fluorophore, Alexa Fluor 647. BCR internalization plots are presented as the negative change in FITC fluorescence relative to that of Alexa Fluor 647, and are calculated as follows:

$$-\frac{\Delta F_{corr}}{F} = -\frac{(I_{FITC} - I_{F0}) - \left[I_{F0} \times \frac{(I_{AF647} - I_{AF0})}{I_{AF0}}\right]}{I_{F0}}$$

Where I_{FITC} is the cell population mean fluorescence intensity (MFI) in the FITC channel at time of measurement, I_{F0} is the initial MFI of the cell population in the FITC channel, I_{AF647} is the cell population MFI in the Alexa Fluor 647 channel at time of measurement, and I_{AF0} is the initial MFI of the cell population in the Alexa Fluor 647 channel.

<u>Total internal reflection fluorescence microscopy (TIRF)</u> – Live cell TIRF microscopy experiments to visualize BCR clusters on the plasma membrane were carried out using DG-75 cells nucleofected (Lonza Kit V, program O-006) with 1.5 µg each of plasmid encoding DG-75 IgM-GFP and mCherry- or RFP-tagged endocytic proteins of interest. Cells were washed into fresh growth medium 24 hours post-transfection and resuspended to a density of 2 million cells/mL. Anti-human IgM Fab'2 was added to a final concentration of 12 µg/mL before a five-minute incubation at 37°C. Stimulated cells were diluted with a four-fold excess of cold imaging buffer (IB: 130 mM NaCl, 2.8 mM KCl, 5 mM $CaCl_2$, 1 mM $MgCl_2$, 10 mM HEPES, 10 mM glucose, pH 7.4), pelleted at 200xg for 5 min, and resuspended in 150 µL of cold imaging buffer. Cleaned, poly-lysine coverslips were rinsed in PBS, assembled with a Warner Instruments coverslip holder (RC-40LP), and the chamber was filled with IB. Approximately 100,000 stimulated, washed cells (50 µL of the final cell suspension) were added to the coverslip, and allowed to settle for 5 minutes prior to dual-color (488 nm and 561 nm excitation) TIRF imaging on an inverted Olympus IX-81 microscope system that has been described in detail previously with a 100x 1.45 NA oil-immersion PlanApo objective (Olympus) and 1.6X optovar, with a DualView beam splitter and an Andor iXon Ultra 897 EM-CCD camera controlled by Andor IQ2 software (Trexler and Taraska, 2017). Typical imaging experiments consisted of 100 ms exposures in each fluorescent channel every second. Registration of

images obtained from excitation at 488 and 561 nm was performed with a custom MATLAB analysis pipeline, using FluoSphere 0.1 µm yellow-green fiducial beads (ThermoFisher F8803) that are visible in both channels. The degree of colocalization between IgM-GFP punctae and the mCherry or RFP-tagged protein of interest was measured by calculating the Pearson correlation coefficient of the pixel intensities surrounding each IgM-GFP cluster in the green and red fluorescence images as previously described (Larson et al., 2014).

Live cell confocal laser scanning microscopy – Imaging of BCR clustering and internalization in live cells in three dimensions was carried out using a Zeiss 880 confocal laser scanning microscope with a 63X, 1.4NA oil-immersion PlanApo DIC objective. DG-75 cells were prepared for imaging by spinning down 1 million cells at 200xg for 5 min, and resuspending the pellet in 100 µL of growth media with 1:1000 anti-human IgM-Fab-Alexa Fluor 488. Fluorescent labeling of the BCR was carried out at 4°C for 30 minutes. Cells were then diluted with 900 µL of imaging buffer, pelleted at 200xg for 5 min, and resuspended in 150 µL IB. Approximately 300,000 labeled cells were allowed to settle for 5 min onto a cleaned, poly-lysine treated, rinsed, coverslip assembled in an Attofluor chamber (ThermoFisher: A7816) imaging chamber containing 600 µL of imaging buffer on a stage heated to 37°C inside an environmental control box. Regions containing multiple live, healthy cells were identified and the equatorial z-position was set as the origin. Two planes above and below this equatorial position were imaged, with a z-step size of 0.43 µm, encompassing a thickness of ~2.1 µM in the middle of the cell. After the addition of anti-human IgM Fab'2 to a final concentration of 12 µg/mL, this five slice stack was imaged once every 6 seconds for a total of 30 min using 488 nm excitation and detecting transmitted and emitted light using T-PMT and GaAsP detectors, respectively.

Immunofluorescence imaging of BCR, actin, and clathrin – To observe endogenous clathrin relative to BCR on the plasma membrane, DG-75 cells were harvested at a concentration of 1-1.5M cells/mL and spun down at 200xg for 5 minutes. The cell pellet was resuspended at 10 million cells/mL in growth medium containing 1:5000 anti-human IgM Fab-Alexa Fluor 594. Cells were labeled for 30 minutes at 4°C followed by a 5-fold dilution in growth medium and centrifugation at 200xg for 5 minutes. The labeled cell pellet was resuspended in growth medium to achieve a density of 2 million cells/mL, and anti-human IgM Fab'2 was added to achieve a Fab'2 concentration of 2 or 8 µg/mL (or omitted for unstimulated cells). Fab'2-stimulated cells were incubated at 37°C for 5 or 15 minutes before diluting the cells 2-fold with cold IB. Approximately 125,000 cells were allowed to settle for 12 minutes onto cleaned, poly-lysine treated, rinsed coverslips in a six-well plate containing 2 mL IB per well. Coverslips were treated with 0.5% paraformaldehyde (PFA) (Electron Microscopy Sciences) in IB for 1 minute before transferring them into 2% PFA in imaging buffer for 20 minutes. Fixed coverslips were washed with PBS, permeabilized by the addition of a solution of 0.5% TritonX-100 and 3% BSA in PBS for 2 minutes, and blocked in a solution of 0.2% TritonX-100 and 3% BSA in PBS for 1 hour. Coverslips were incubated in primary mouse anti-clathrin heavy chain antibody X-22 (6 µg/mL in blocking buffer) for 1 hour, washed with blocking buffer, and incubated with secondary donkey anti-mouse-Alexa Fluor 647 antibody (2 µg/mL) and phalloidin-Alexa Fluor 488 (33 nM) in blocking buffer for 1 hour. After washing in blocking buffer and PBS, coverslips were fixed for 10 minutes in 2% PFA in PBS, rinsed in PBS, and stored

at 4°C protected from light until imaging. Fixed, immunostained cells were imaged on the same Zeiss 880 confocal laser scanning microscope setup used for live cell imaging, using a 3-track program with excitation at 488, 561, and 633 nm. Z-stacks were collected to encompass the full cell volume.

Direct stochastic optical reconstruction microscopy (dSTORM) – The super-resolution localization method, dSTORM, was used to measure nanoscale changes in the size of BCR clusters on the plasma membrane following stimulation with anti-human IgM Fab'2. DG-75 cells were prepared for imaging exactly as described for immunofluorescence imaging, but labeled with anti-human IgM Fab-Alexa Fluor 647 (1:5000 in growth medium) and without permeabilization or additional staining for clathrin or actin. Fixed, PBS washed coverslips were assembled in sealed AttoFluor imaging chambers (Thermo Fisher) containing a freshly-prepared dSTORM buffer (10% w/v D-glucose, 100 mM beta-mercaptoethanol, 0.8 mg/mL glucose oxidase, and 0.04 mg/mL catalase in PBS). Imaging was carried out as previously described in detail using a Nikon Eclipse Ti inverted microscope with a 100X, 1.49NA objective, and an Andor iXon Ultra 897 EM-CCD camera under the control of Nikon Elements NSTORM software (Sochacki and Taraska, 2017). STORM imaging was performed in TIRF, with 647 nm excitation at 75% laser power, collecting 10-20,000 frames with 10 msec exposure times. STORM images were processed as described previously, with the following modifications: a minimum height of 200 was used in the identification parameters for all images, and a value of 200 was used as the minimum number of photons during filtering. Drift correction was performed in Nikon Elements software, and Tiff images were rendered using a cross representation with 8 nm pixel size. Localization precision was measured using fourier shell correlation and measurement of individual localizations in the rendered Tiff image files, both of which yielded an apparent precision of ~27 nm.

In order to measure BCR cluster sizes from the STORM data, images were maximum filtered using a radius of 1 pixel (8 nm), and thresholded using the Li filter in Fiji/ImageJ (Schindelin et al., 2012) to produce a down-sampled, binary image, with a resolution of 40 nm. The result of this processing is to cluster localizations that are separated in space by a distance of less than the precision of the original image, 24 nm, edge-to-edge – a conservative distance cutoff, which was empirically determined to identify reasonable clusters across the conditions tested i.e. monodisperse, small punctae in unstimulated cells, and heterogeneous, larger cluster sizes in stimulated cells. Six to twelve cells were analyzed for each condition, and the areas of all particles in the thresholded images were measured in Fiji/ImageJ. The total fluorescent area was measured for each cell, and the percent of this area composed of small (<9600 nm^2), intermediate (9600 – 48000 nm^2), and large (>48000 nm^2) fluorescent punctae was plotted in Origin (OriginLab). As described in the results section, these area cutoffs were selected based on the typical size of clathrin coated pits.

Correlative super-resolution fluorescence and electron microscopy – In order to directly visualize endocytic structures associated with BCR fluorescence, DG-75 cells were prepared for imaging exactly as described for STORM imaging above, with a few modifications. After 12 minutes of attachment to poly-L-lysine coated gold fiducial coverslips (Hestzig, LLC) cells were fixed and 'unroofed' in order to expose the cytoplasmic surface of the membrane adhered to the coverslip by squirting 4 mL of 0.75% PFA in stabilization buffer (70 mM KCl, 5 mM $MgCl_2$, 30 mM HEPES, pH 7.4) steadily onto each coverslip using a

10-mL syringe with a 21Gx1.5 needle, moving the stream over the coverslip at a right angle. After unroofing, coverslips were fixed in 2% PFA in stabilization buffer for 20 minutes, rinsed with PBS, treated with phalloidin-Alexa Fluor 488 (33 nM in PBS) for 10 minutes, and rinsed again in PBS prior to imaging.

Labeled, unroofed coverslips were assembled in sealed AttoFluor chambers containing freshly prepared dSTORM buffer. Imaging was performed as described above, with some additional steps to map cells on the coverslip for later correlation with TEM images. As described elsewhere (Sochacki et al., 2017), a ~1mm^2 region of the coverslip was initially mapped by montaging a 15x15 area in epifluorescence with excitation at 488 and 647 nm. These large montages of the phalloidin-Alexa Fluor 488 label were useful for re-identification of the cells imaged by STORM prior to imaging platinum replicas by TEM. After imaging 5-8 cells, a 4 mm diameter circle was etched on the bottom of the coverslip with a diamond objective (Leica) to indicate the area of interest during sample processing for EM. Etched coverslips were cleaned of oil and fixed in a 2% solution of glutaraldehyde in PBS (Electron Microscopy Sciences).

As described previously (Sochacki et al., 2017) coverslips were prepared for EM by treatment with 0.1% tannic acid solution for 20 min, rinsing with water, and staining with 0.1% uranyl acetate for 20 minutes. Coverslips were dehydrated using a Tousimis critical point dryer, and coated with platinum and carbon in a JEOL freeze fracture device (Sochacki et al., 2012). After locating cells of interest under a 10X phase-contrast objective, carbon-platinum replicas were separated from the underlying glass coverslip using 5% hydrofluoric acid, and lifted onto glow-discharged formvar-coated 75 mesh copper grids for imaging on a JEOL 1400 TEM using SerialEM software for montaging (Mastronarde, 2005), at a magnification of 15,000x.

STORM images were processed as described above, but Tiff images were rendered using a Gaussian representation with 8 nm pixel size. STORM image files were transformed using custom MATLAB software to align images based on the measured coordinates of gold nanorods visible in both the rendered dSTORM Tiff files and TEM montages.

DG-75 plasma membrane ferritin labeling

49 mg of cationized ferritin from horse spleen (Sigma-Aldrich F1897) was sonicated for 10-15 seconds and then added to three million DG-75 cells for each condition. Samples were then gently swirled by hand to disperse ferritin. Next, the samples were incubated on ice for 10 minutes to allow the ferritin to adhere to cell membranes and then warmed at 37°C for 30 seconds. The samples were spun in a mini-centrifuge in 10 second interval bursts to produce a pellet of approximately 2 mm x 3 mm. The unstimulated sample was then immediately fixed with 2.5% glutaraldehyde and 1% paraformaldehyde in 0.12 M sodium cacodylate buffer at pH 7.2 for 1 hour at room temperature. The stimulated sample was resuspended in PBS and administered Fab'2 at a final concentration of 8 µg/ml and incubated for 15 minutes at 37°C. After incubation, stimulated cells were fixed in the same manner described for the unstimulated sample.

Thin-section transmission electron microscopy

Fixed samples were washed 3 times (20 minutes each) with 0.12 M sodium cacodylate buffer and stained with 1% osmium tetroxide (on ice and in the dark) for 1 hour, washed twice (10 minutes each) in water, and stained with 1% uranyl acetate (overnight at 4°C). The following day samples were processed through a dehydration protocol of increasing concentrations of ethanol, infiltrated with Epon resin, and polymerized at 60°C for at least 48 hours (VWR Symphony oven). Post-staining was determined to be not necessary due to sufficient contrast observed for ferritin. 65-70 nm ultrathin sections were obtained on a Leica-Reichert Ultracut microtome with a diamond knife (Delaware Diamond Knives, Inc.) after each sample block resin was trimmed by a glass knife, and confirmed to be in the cell layer through thick sectioning and Toluidene blue dye. Ultrathin sections were imaged on 200 mesh grids in a JEOL 1400 TEM.

Analysis of EM and CLEM images

Platinum replica EM images of the entire visible plasma membrane of each cell were segmented by hand using ImageJ/FIJI with ROIs corresponding to the 1) total plasma membrane area, 2) clathrin-coated structures, 3) smooth-raised membranes, and 4) gold fiducial particles. These ROIs were used to calculate density of structures, area of individual structures, Feret's diameter of single structures, and nearest-neighbor distances between structures. Analysis, statistics, and plotting were done in Origin (OriginLab). The overlap pixel area between clathrin structures and SRMs was calculated from image masks made from ROIs in Matlab (MathWorks).

The distribution and density of super-resolution dSTORM fluorescence signal excluding regions 0.5 micron radius from gold fiducials were analyzed using the above EM identified clathrin/SRM segmentation masks. Fluorescence signal within and surrounding a 200 nm radius of each segmented membrane structure was measured against the total fluorescence in the surrounding 1.8 micron radius area using Matlab. The resulting fluorescence ratio measurements for each structure in all experimental conditions were plotted in Origin (Originlab).

AUTHOR CONTRIBUTIONS: TMD and JWT designed experiments. TMD performed molecular biology, confocal, FACS, and TIRF experiments. TMD, AMD, and KAS performed platinum replica TEM and CLEM experiments. KAS designed and wrote analysis software. RA and ADR did thin section TEM. TMD and JWT wrote the manuscript and all authors commented on work. JWT oversaw the project.

ACKNOWLEDGMENTS: We would like to thank the NHLBI Electron Microscopy core for support with EM imaging and instrumentation, Xufeng Wu and the NHLBI light Microscopy core for support with fluorescence imaging and instrumentation, the NHLBI FACS core for support with flow cytometry, and all members of the Taraska lab for comments and scientific dialogue. We would like to thank Agila Somasundaram for critically reading the manuscript. We would like to thank Ethan Tyler of NIH Medical Arts for illustration work on the model figure. JWT is supported by the NHLBI Intramural Research Program, National Institutes of Health, Bethesda, Maryland.

FIGURE LEGENDS

Figure 1. BCR internalization in human DG-75 cells. (a) Confocal images of a live DG-75 cell labeled with anti-human IgM Fab-Alexa Fluor 488 and stimulated with 12 µg/ml of anti-human IgM Fab'2 at t = 0 min. BCR is shown in green and transmitted light is grayscale. Scale bar = 5 µm. (b) Upper left region of cell in (a); magenta arrow tracks BCRs that cluster and internalize into the cytoplasm. Scale bar is 2 µm. (c) Diagram of flow-cytometry assay of BCR internalization in DG-75 cells following the addition of Fab'2. (d) Plot of BCR internalization measured by the change in fluorescence of anti-human IgM Fab FITC relative to the change in fluorescence of anti-human IgM Fab Alexa Fluor 647 over time following the addition of anti-human IgM Fab'2 at concentrations ranging from 0-14 µg/mL. (e) Plot of BCR internalization at 60 min of stimulation as a function of varying concentrations of anti-human IgM Fab'2. Error in (d) and (e) indicate standard deviation across five experiments. (f) Colocalization of BCR and clathrin in immunofluorescence confocal images of DG-75 cells labeled with anti-human IgM Fab-Alexa Fluor 488 (green) and stimulated with either 2 or 8 µg/mL of Fab'2 for 5 min prior fixation and staining for clathrin (magenta). Scale bars are 2 µm. Zoomed images for each treatment on right are from yellow boxes on left. (g) Extracted and averaged images of single Fab'2-induced IgM-GFP spots (cyan) at the plasma membrane and 10 different red-labeled endocytic proteins (magenta) expressed in live DG-75 cells imaged by two-color TIRF. Scale bar is 2 µm. The corresponding Pearson's correlation values between image pairs are shown below for each protein. Plots show the mean (square), median (line), 25/75 percentile range (box), and outliers with a coefficient value of 1.5. n = AP2beta, 15 cells, 349 spots; CLC, 16 cells, 392 spots; Epsin1, 10 cells, 298 spots; HIP1R, 12 cells, 414 spots; Eps15, 11 cells, 300 spots; CALM, 11 cells, 287 spots; FCHO1, 12 cells, 222 spots; Dyn2, 15 cells, 556 spots; 222 spots; TFR, 14 cells, 389 spots; LifeAct, 5 cells, 396 spots.

Figure 2. Super-resolution dSTORM imaging of Fab'2-induced BCR clustering on the membrane of DG-75 cells. (a) Reconstructed super-resolution images of BCR (magenta) clustering on the bottom surface of DG-75 cells labeled with anti-human IgM Fab-Alexa Fluor 647 and left unstimulated or stimulated with anti-human IgM Fab'2 at either 2 or 8 µg/mL Fab'2 for 15 min prior to plating, fixation, and imaging. Scale bar is 5 µm. (b) Percent of total fluorescent area in each cell composed of small (<9600 nm^2, orange bar), intermediate (9600-48000 nm^2, magenta bar), and large (> 48000 nm^2, blue bar) punctae for unstimulated DG-75 cells, cells stimulated with 2 µg/mL Fab'2 for 5 or 15 minutes, and cells stimulated with 8 µg/mL Fab'2 for 5 or 15 minutes (n = unstim. 11 cells – 32,797 spots, 5 min 2 µg/ml 10 cells – 23,728 spots, 5 min 8 µg/ml 12 cells – 10,497 spots, 15 min 2 µg/ml 9 cells – 14,347 spots, 15 min 8 µg/ml 8 cells – 5,034 spots). Plots show the mean (square), median (line), 25/75 percentile range (box), and outliers with a coefficient value of 1.5 and data points (black) from each cell.

Figure 3. Correlative light and electron microscopy (CLEM) imaging of unstimulated DG-75 cells. (a) Reconstructed dSTORM image of a DG-75 cell labeled with anti-human IgM Fab-Alexa Fluor 647 prior to plating, fixation, and unroofing. Scale bar is 5 µm. (b) Platinum replica transmission electron microscopy (PREM) image of the cytoplasmic surface of the plasma membrane from (a). Scale bar is 5 µm. (c) CLEM overlay of images of (a) and (b). Scale bar is 5 µm. (d) Zoom of region from (c, yellow box). Scale bar is 1 µm.

Figure 4. CLEM analysis of membrane changes during BCR clustering 5 minutes post Fab'2 stimulation. Representative CLEM images of DG-75 cells treated for 5 min with 2 µg/mL (a-d) or 8 µg/mL (e-h) Fab'2. Reconstructed STORM images (a and e). PREM image of the cytoplasmic surface of the cells shown in a and e (b and f). CLEM overlay images (c and g). Scale Bars 5 µm. Zoomed regions from c and g (yellow boxes) show differences in BCR clustering and membrane morphology changes between the two concentrations of Fab'2 (d and h). Scale bar is 1 µm.

Figure 5. CLEM analysis of membrane morphological changes during BCR clustering 15 minutes post Fab'2 stimulation. Representative CLEM images of DG-75 cells treated for 15 min with 2 µg/mL (a-d) or 8 µg/mL (e-h) Fab'2 prior to analysis. Reconstructed STORM image (a and e). PREM images of the cytoplasmic surface of the cells shown in a and e (b and f). White regions are grid bars. CLEM overlay images (c and g). Scale Bars 5 µm. Zoomed regions from C and G (yellow boxes) show differences in BCR clustering and membrane changes between the two treatments. Clathrin-like honeycomb structures can be observed associated with smooth raised portions of the membrane in the 8 µg/mL Fab'2 samples. These structures are rarely found in cells treated with 2 µg/mL Fab'2 (d and h). Scale bar is 1 µm.

Figure 6. Changes in clathrin and smooth raised membrane structures in TEM images following Fab'2 stimulation. (a) Representative PREM images of clathrin (left), smooth raised membrane (SRM) structures (center), and clathrin on SRMs (right). Scale bars are 100 nm. (b) Example PREM image used for identification and resulting segmentation shown for (c) clathrin marked in yellow, (d) smooth raised membrane structures as blue objects, and (e) an overlay with the clathrin found on SRM structures as white regions. These segmented masks were used to measure (f) the change in the density of CCS on the membrane, (g) changes in CCS radius, and (h) the nearest-neighbor distances between CCS (n = Unstim. 5 cells, 222 ccs structures, 5 min 2 µg/ml 9 cells, 486 ccs structures, 5 min 8 µg/ml 6 cells, 482 ccs structures, 15 min 2 µg/ml 6 cells, 499 ccs structures, 15 min 8 µg/ml 6 cells, 728 ccs structures). The same measurements for SRM density (i), SRM radius (j), and nearest-neighbor distance (k) (n = Unstim. 5 cells, 326 SRM structures, 5 min 2 µg/ml 9 cells, 553 SRM structures, 5 min 8 µg/ml 6 cells, 313 SRM structures, 15 min 2 µg/ml 6 cells, 368 SRM structures, 15 min 8 µg/ml 6 cells, 639 SRM structures). Association of CCS and SRM structures were quantified in (l). Nearly all CCS were found on SRM in cells stimulated for 15 min with 8 µg/mL Fab'2. Box and whisker plots show the mean (square), median (line), 25/75 percentile range (box), and outliers with a coefficient value of 1.5 for same cells from f-k.

Figure 7. Analysis of changes in the distribution of BCR fluorescence relative to CCS and SRM structures in CLEM images following Fab'2 stimulation. The fraction of BCR fluorescence measured in an 1800 nm total radius located within 200 nm of a (a) CCS (b) SRM or (c) Clathrin on SRMs for 5 different experimental conditions measured from CLEM images. After 5 minutes of stimulation with 8 µg/mL Fab'2, approximately 70% of all BCR fluorescence is found within 200 nm of CCS, and after 15 minutes of stimulation with 8 µg/mL of Fab'2 nearly 80% of all BCR fluorescence is found within 200 nm of clathrin on SRM structures. Bar graph shows mean +/- SD (n = Unstim. 5 cells, 5 min 2 µg/ml 9 cells, 5 min 8 µg/ml 6 cells, 15 min 2 µg/ml 6 cells, 15 min 8 µg/ml 6 cells).

Figure 8. Model of BCR clustering and internalization following stimulation with anti-human IgM Fab'2 at different concentrations. (a) At low concentrations of Fab'2, BCR crosslinking is less favorable and BCR clusters remain small on the cell surface. These small clusters may be internalized by classical clathrin mediated endocytosis. (b) Higher concentrations of Fab'2 generate larger BCR clusters. In this case, larger clusters may not be readily internalized by small clathrin-coated structures but rely on clathrin to cluster and organize BCRs and then bulk membrane remodeling to capture large pieces of the membrane containing BCRs and clathrin into the cytoplasm. Clathrin-coated vesicles may then bud directly from these membranes while they are attached to the plasma membrane or after scission from the plasma membrane to recycle or process receptor complexes.

Supplementary Figure 1. BCR capping in human DG-75 cells after antigen activation. (a) Representative confocal images of a live DG-75 cell labeled with anti-human IgM Fab-Alexa Fluor 488 and stimulated with 8 µg/ml of anti-human IgM Fab'2 at t = 0 minutes. Labeled BCR is shown in green and transmitted light is grayscale. Scale bar = 5 µm. BCR is seen to accumulate and form a cap at one pole of the cell (magenta arrow).

Supplementary Figure 2. TEM analysis the resting B cell plasma membrane. (a-c) Representative thin-section TEM images of DG-75 cells treated with extracellular cationized ferritin (15 nm black dots) to label the outer leaflet of the plasma membrane and the inner leaflet of endocytic carriers (Scale Bars 1 µm). Zoomed regions from cells shown in a-c (colored boxes) show details of membrane morphology. Scale bar is 100 nm.

Supplementary Figure 3. TEM analysis of membrane morphological changes during BCR clustering 15 minutes post Fab'2 stimulation in B cells. (a) Representative thin-section TEM images of DG-75 cells treated with extracellular cationic ferritin (15 nm black dots) to label the outer leaflet of the plasma membrane and the inner leaflet of endocytic carriers and 8 µg/mL Fab'2 for 15 minutes to activate and cluster BCRs. Scale Bar is 1 µm. (b,c) Two zoomed regions (colored boxes) from the same cell shown in (a) show details of membrane morphology of large endocytic carriers that take up ferritin. Scale bar is 100 nm. Two additional stimulated cells and zoomed regions (colored boxes) are shown in d-g. Scale bars are 1 µm and 100 nm.

REFERENCES

Avalos, A.M., Meyer-Wentrup, F., and Ploegh, H.L. (2014). B-cell receptor signaling in lymphoid malignancies and autoimmunity. Adv Immunol *123*, 1-49.
Batista, F.D., Iber, D., and Neuberger, M.S. (2001). B cells acquire antigen from target cells after synapse formation. Nature *411*, 489-494.
Betzig, E., Patterson, G.H., Sougrat, R., Lindwasser, O.W., Olenych, S., Bonifacino, J.S., Davidson, M.W., Lippincott-Schwartz, J., and Hess, H.F. (2006). Imaging intracellular fluorescent proteins at nanometer resolution. Science *313*, 1642-1645.
Brown, B.K., and Song, W. (2001). The actin cytoskeleton is required for the trafficking of the B cell antigen receptor to the late endosomes. Traffic *2*, 414-427.

Chapman, C.J., Zhou, J.X., Gregory, C., Rickinson, A.B., and Stevenson, F.K. (1996). VH and VL gene analysis in sporadic Burkitt's lymphoma shows somatic hypermutation, intraclonal heterogeneity, and a role for antigen selection. Blood *88*, 3562-3568.
Cheng, P.C., Dykstra, M.L., Mitchell, R.N., and Pierce, S.K. (1999). A role for lipid rafts in B cell antigen receptor signaling and antigen targeting. J Exp Med *190*, 1549-1560.
Clark, M.R., Massenburg, D., Siemasko, K., Hou, P., and Zhang, M. (2004). B-cell antigen receptor signaling requirements for targeting antigen to the MHC class II presentation pathway. Curr Opin Immunol *16*, 382-387.
Cleyrat, C., Darehshouri, A., Anderson, K.L., Page, C., Lidke, D.S., Volkmann, N., Hanein, D., and Wilson, B.S. (2013). The architectural relationship of components controlling mast cell endocytosis. J Cell Sci *126*, 4913-4925.
Conner, S.D., and Schmid, S.L. (2003). Regulated portals of entry into the cell. Nature *422*, 37-44.
Dambournet, D., Sochacki, K.A., Cheng, A.T., Akamatsu, M., Taraska, J.W., Hockemeyer, D., and Drubin, D.G. (2018). Genome-edited human stem cells expressing fluorescently labeled endocytic markers allow quantitative analysis of clathrin-mediated endocytosis during differentiation. J Cell Biol.
Davis, R.E., Ngo, V.N., Lenz, G., Tolar, P., Young, R.M., Romesser, P.B., Kohlhammer, H., Lamy, L., Zhao, H., Yang, Y.*, et al.* (2010). Chronic active B-cell-receptor signalling in diffuse large B-cell lymphoma. Nature *463*, 88-92.
Ferreira, A.P.A., and Boucrot, E. (2018). Mechanisms of Carrier Formation during Clathrin-Independent Endocytosis. Trends Cell Biol *28*, 188-200.
Harding, C., Heuser, J., and Stahl, P. (1983). Receptor-mediated endocytosis of transferrin and recycling of the transferrin receptor in rat reticulocytes. J Cell Biol *97*, 329-339.
Harwood, N.E., and Batista, F.D. (2010). Early events in B cell activation. Annu Rev Immunol *28*, 185-210.
Heilemann, M., van de Linde, S., Schuttpelz, M., Kasper, R., Seefeldt, B., Mukherjee, A., Tinnefeld, P., and Sauer, M. (2008). Subdiffraction-resolution fluorescence imaging with conventional fluorescent probes. Angew Chem Int Ed Engl *47*, 6172-6176.
Hoogeboom, R., and Tolar, P. (2016). Molecular Mechanisms of B Cell Antigen Gathering and Endocytosis. Curr Top Microbiol Immunol *393*, 45-63.
Kopek, B.G., Paez-Segala, M.G., Shtengel, G., Sochacki, K.A., Sun, M.G., Wang, Y., Xu, C.S., van Engelenburg, S.B., Taraska, J.W., Looger, L.L.*, et al.* (2017). Diverse protocols for correlative super-resolution fluorescence imaging and electron microscopy of chemically fixed samples. Nat Protoc *12*, 916-946.
Larson, B.T., Sochacki, K.A., Kindem, J.M., and Taraska, J.W. (2014). Systematic spatial mapping of proteins at exocytic and endocytic structures. Mol Biol Cell *25*, 2084-2093.
Lee, J., Sengupta, P., Brzostowski, J., Lippincott-Schwartz, J., and Pierce, S.K. (2017). The nanoscale spatial organization of B-cell receptors on immunoglobulin M- and G-expressing human B-cells. Mol Biol Cell *28*, 511-523.
Mastronarde, D.N. (2005). Automated electron microscope tomography using robust prediction of specimen movements. J Struct Biol *152*, 36-51.
Matsuda, F., Shin, E.K., Nagaoka, H., Matsumura, R., Haino, M., Fukita, Y., Taka-ishi, S., Imai, T., Riley, J.H., Anand, R.*, et al.* (1993). Structure and physical map of 64 variable segments in the 3'0.8-megabase region of the human immunoglobulin heavy-chain locus. Nat Genet *3*, 88-94.
Mayor, S., Parton, R.G., and Donaldson, J.G. (2014). Clathrin-independent pathways of endocytosis. Cold Spring Harb Perspect Biol *6*.
McMahon, H.T., and Boucrot, E. (2011). Molecular mechanism and physiological functions of clathrin-mediated endocytosis. Nat Rev Mol Cell Biol *12*, 517-533.

Mettlen, M., Chen, P.H., Srinivasan, S., Danuser, G., and Schmid, S.L. (2018). Regulation of Clathrin-Mediated Endocytosis. Annu Rev Biochem *87*, 871-896.
Natkanski, E., Lee, W.Y., Mistry, B., Casal, A., Molloy, J.E., and Tolar, P. (2013). B cells use mechanical energy to discriminate antigen affinities. Science *340*, 1587-1590.
Onabajo, O.O., Seeley, M.K., Kale, A., Qualmann, B., Kessels, M., Han, J., Tan, T.H., and Song, W. (2008). Actin-binding protein 1 regulates B cell receptor-mediated antigen processing and presentation in response to B cell receptor activation. J Immunol *180*, 6685-6695.
Pierce, S.K., and Liu, W. (2010). The tipping points in the initiation of B cell signalling: how small changes make big differences. Nat Rev Immunol *10*, 767-777.
Salisbury, J.L., Condeelis, J.S., and Satir, P. (1980). Role of coated vesicles, microfilaments, and calmodulin in receptor-mediated endocytosis by cultured B lymphoblastoid cells. J Cell Biol *87*, 132-141.
Schindelin, J., Arganda-Carreras, I., Frise, E., Kaynig, V., Longair, M., Pietzsch, T., Preibisch, S., Rueden, C., Saalfeld, S., Schmid, B*., et al.* (2012). Fiji: an open-source platform for biological-image analysis. Nat Methods *9*, 676-682.
Scott, B.L., Sochacki, K.A., Low-Nam, S.T., Bailey, E.M., Luu, Q., Hor, A., Dickey, A.M., Smith, S., Kerkvliet, J.G., Taraska, J.W*., et al.* (2018). Membrane bending occurs at all stages of clathrin-coat assembly and defines endocytic dynamics. Nat Commun *9*, 419.
Sezgin, E., Levental, I., Mayor, S., and Eggeling, C. (2017). The mystery of membrane organization: composition, regulation and roles of lipid rafts. Nat Rev Mol Cell Biol *18*, 361-374.
Sigismund, S., Argenzio, E., Tosoni, D., Cavallaro, E., Polo, S., and Di Fiore, P.P. (2008). Clathrin-mediated internalization is essential for sustained EGFR signaling but dispensable for degradation. Dev Cell *15*, 209-219.
Siraganian, R.P., de Castro, R.O., Barbu, E.A., and Zhang, J. (2010). Mast cell signaling: the role of protein tyrosine kinase Syk, its activation and screening methods for new pathway participants. FEBS Lett *584*, 4933-4940.
Sochacki, K.A., Dickey, A.M., Strub, M.P., and Taraska, J.W. (2017). Endocytic proteins are partitioned at the edge of the clathrin lattice in mammalian cells. Nat Cell Biol *19*, 352-361.
Sochacki, K.A., Larson, B.T., Sengupta, D.C., Daniels, M.P., Shtengel, G., Hess, H.F., and Taraska, J.W. (2012). Imaging the post-fusion release and capture of a vesicle membrane protein. Nat Commun *3*, 1154.
Sochacki, K.A., Shtengel, G., van Engelenburg, S.B., Hess, H.F., and Taraska, J.W. (2014). Correlative super-resolution fluorescence and metal-replica transmission electron microscopy. Nat Methods *11*, 305-308.
Sochacki, K.A., and Taraska, J.W. (2017). Correlative Fluorescence Super-Resolution Localization Microscopy and Platinum Replica EM on Unroofed Cells. Methods Mol Biol *1663*, 219-230.
Souwer, Y., Griekspoor, A., Jorritsma, T., de Wit, J., Janssen, H., Neefjes, J., and van Ham, S.M. (2009). B cell receptor-mediated internalization of salmonella: a novel pathway for autonomous B cell activation and antibody production. J Immunol *182*, 7473-7481.
Srinivas Reddy, A., Tsourkas, P.K., and Raychaudhuri, S. (2011). Monte Carlo study of B-cell receptor clustering mediated by antigen crosslinking and directed transport. Cell Mol Immunol *8*, 255-264.
Stoddart, A., Jackson, A.P., and Brodsky, F.M. (2005). Plasticity of B cell receptor internalization upon conditional depletion of clathrin. Mol Biol Cell *16*, 2339-2348.
Stone, M.B., Shelby, S.A., Nunez, M.F., Wisser, K., and Veatch, S.L. (2017). Protein sorting by lipid phase-like domains supports emergent signaling function in B lymphocyte plasma membranes. Elife *6*.
Taylor, M.J., Perrais, D., and Merrifield, C.J. (2011). A high precision survey of the molecular dynamics of mammalian clathrin-mediated endocytosis. PLoS Biol *9*, e1000604.

Thyagarajan, R., Arunkumar, N., and Song, W. (2003). Polyvalent antigens stabilize B cell antigen receptor surface signaling microdomains. J Immunol *170*, 6099-6106.
Tolar, P. (2017). Cytoskeletal control of B cell responses to antigens. Nat Rev Immunol *17*, 621-634.
Tomas, A., Futter, C.E., and Eden, E.R. (2014). EGF receptor trafficking: consequences for signaling and cancer. Trends Cell Biol *24*, 26-34.
Trexler, A.J., and Taraska, J.W. (2017). Two-Color Total Internal Reflection Fluorescence Microscopy of Exocytosis in Endocrine Cells. Methods Mol Biol *1563*, 151-165.
Trombetta, E.S., and Mellman, I. (2005). Cell biology of antigen processing in vitro and in vivo. Annu Rev Immunol *23*, 975-1028.
Watanabe, S., and Boucrot, E. (2017). Fast and ultrafast endocytosis. Curr Opin Cell Biol *47*, 64-71.
Wilson, B.S., Pfeiffer, J.R., and Oliver, J.M. (2002). FcepsilonRI signaling observed from the inside of the mast cell membrane. Mol Immunol *38*, 1259-1268.
Zhu, Q., Zhang, M., Shi, M., Liu, Y., Zhao, Q., Wang, W., Zhang, G., Yang, L., Zhi, J., Zhang, L.*, et al.* (2016). Human B cells have an active phagocytic capability and undergo immune activation upon phagocytosis of Mycobacterium tuberculosis. Immunobiology *221*, 558-567.

Figure 1

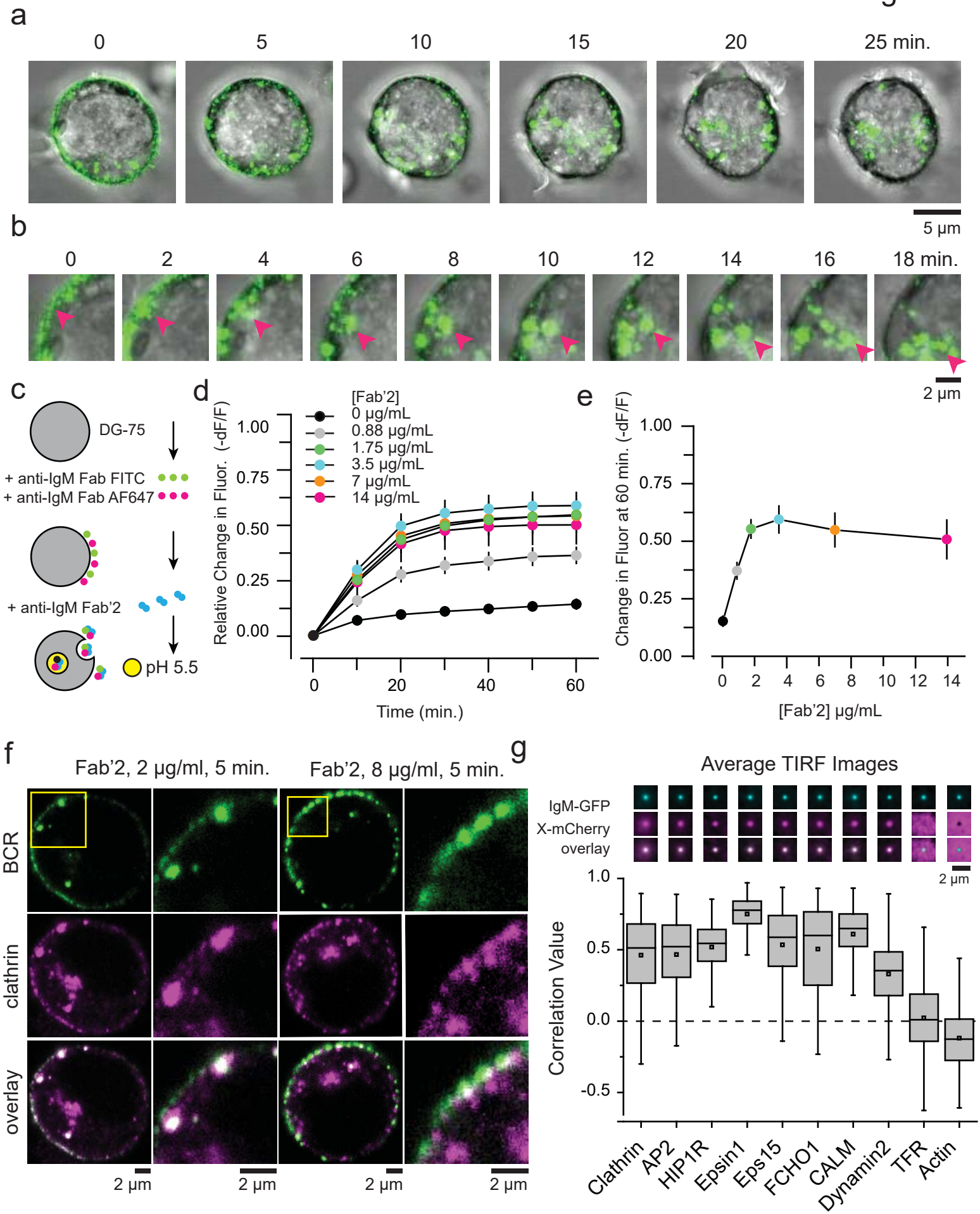
a
0
5
10
15
20
25 min.
5 µm
b
0
2
4
6
8
10
12
14
16
18 min.
2 µm
c
DG-75
+ anti-IgM Fab FITC
+ anti-IgM Fab AF647
+ anti-IgM Fab'2
pH 5.5
d
[Fab'2]
0 µg/mL
0.88 µg/mL
1.75 µg/mL
3.5 µg/mL
7 µg/mL
14 µg/mL
Relative Change in Fluor. (-dF/F)
1.00
0.75
0.50
0.25
0.00
0
20
40
60
Time (min.)
e
Change in Fluor at 60 min. (-dF/F)
1.00
0.75
0.50
0.25
0.00
0
2
4
6
8
10
12
14
[Fab'2] µg/mL
f
Fab'2, 2 µg/ml, 5 min.
Fab'2, 8 µg/ml, 5 min.
BCR
clathrin
overlay
2 µm
2 µm
2 µm
2 µm
g
Average TIRF Images
IgM-GFP
X-mCherry
overlay
2 µm
Correlation Value
1.0
0.5
0.0
-0.5
Clathrin
AP2
HIP1R
Epsin1
Eps15
FCHO1
CALM
Dynamin2
TFR
Actin

Figure 2

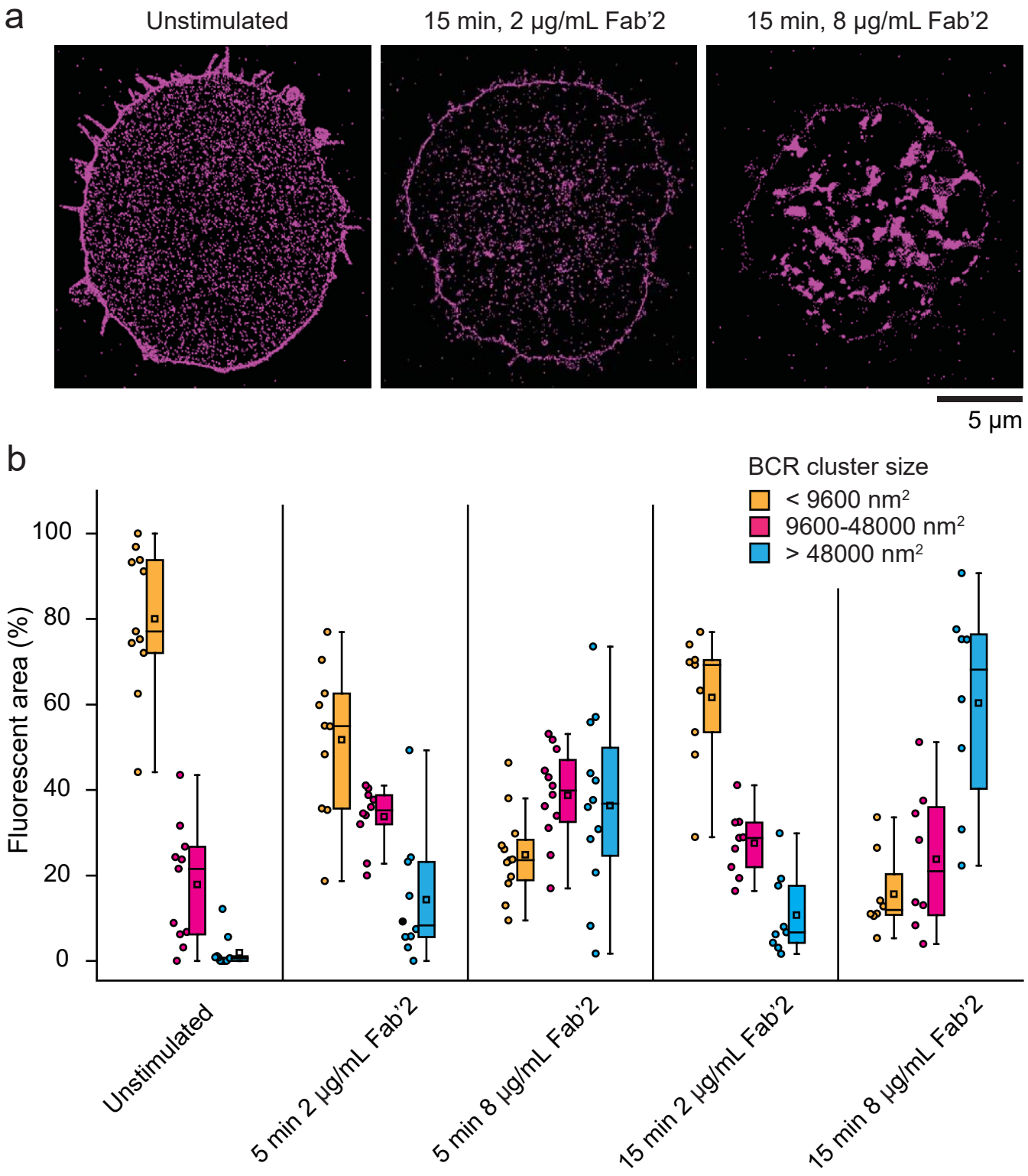
a
Unstimulated
15 min, 2 µg/mL Fab'2
15 min, 8 µg/mL Fab'2
5 µm
b
BCR cluster size
< 9600 nm²
9600-48000 nm²
> 48000 nm²
Fluorescent area (%)
0
20
40
60
80
100
Unstimulated
5 min 2 µg/mL Fab'2
5 min 8 µg/mL Fab'2
15 min 2 µg/mL Fab'2
15 min 8 µg/mL Fab'2

Figure 3

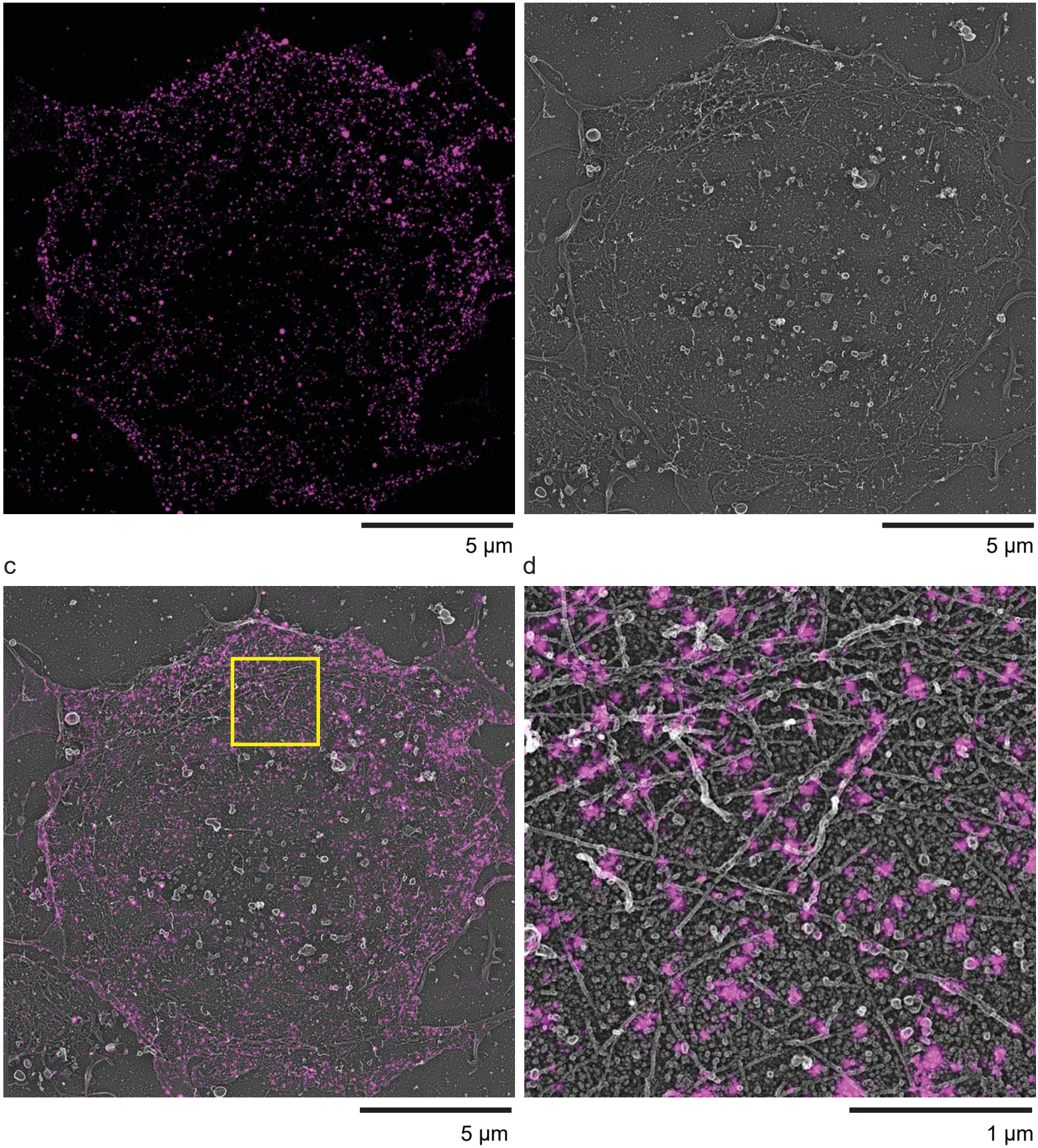

Figure 4

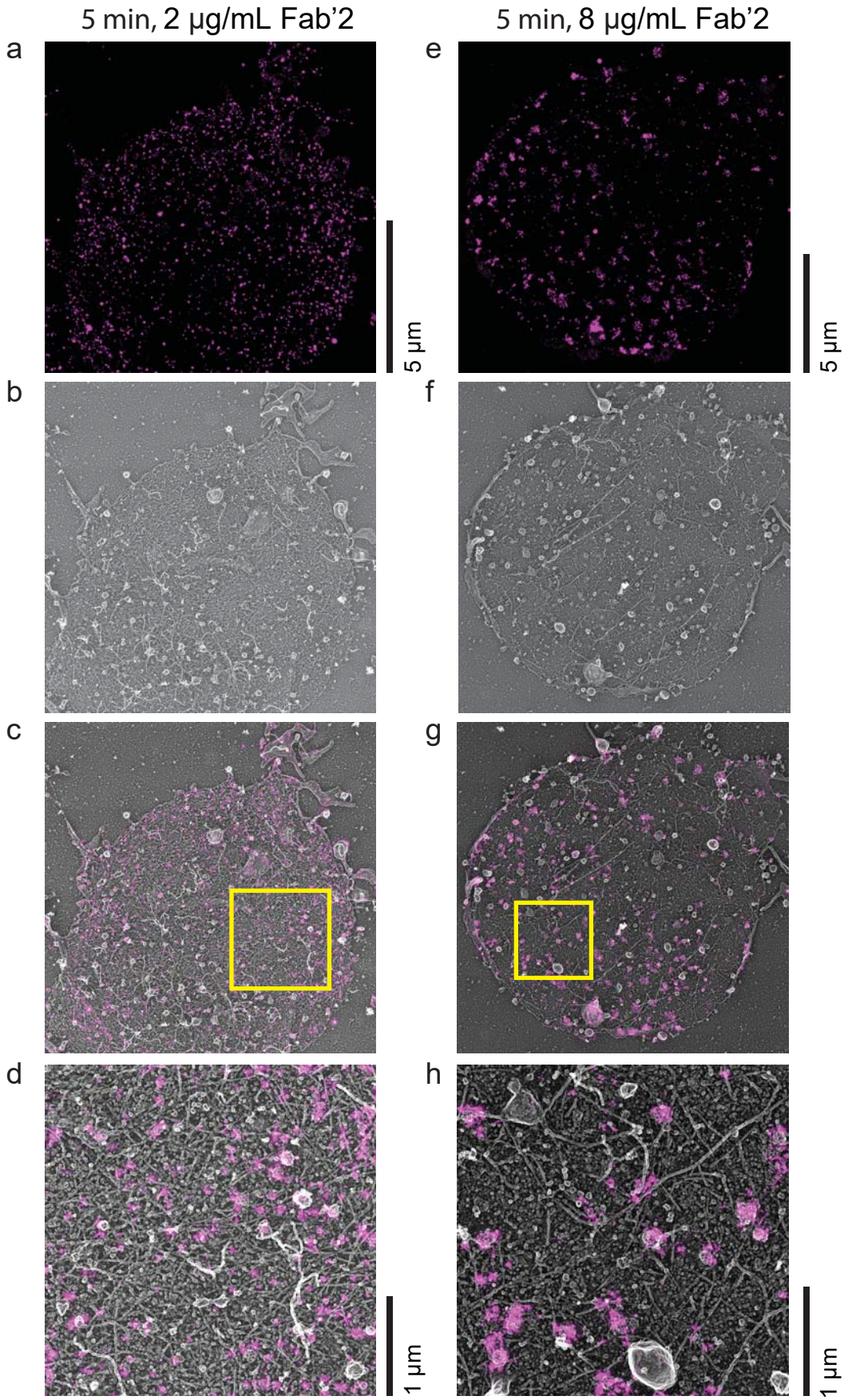

Figure 5

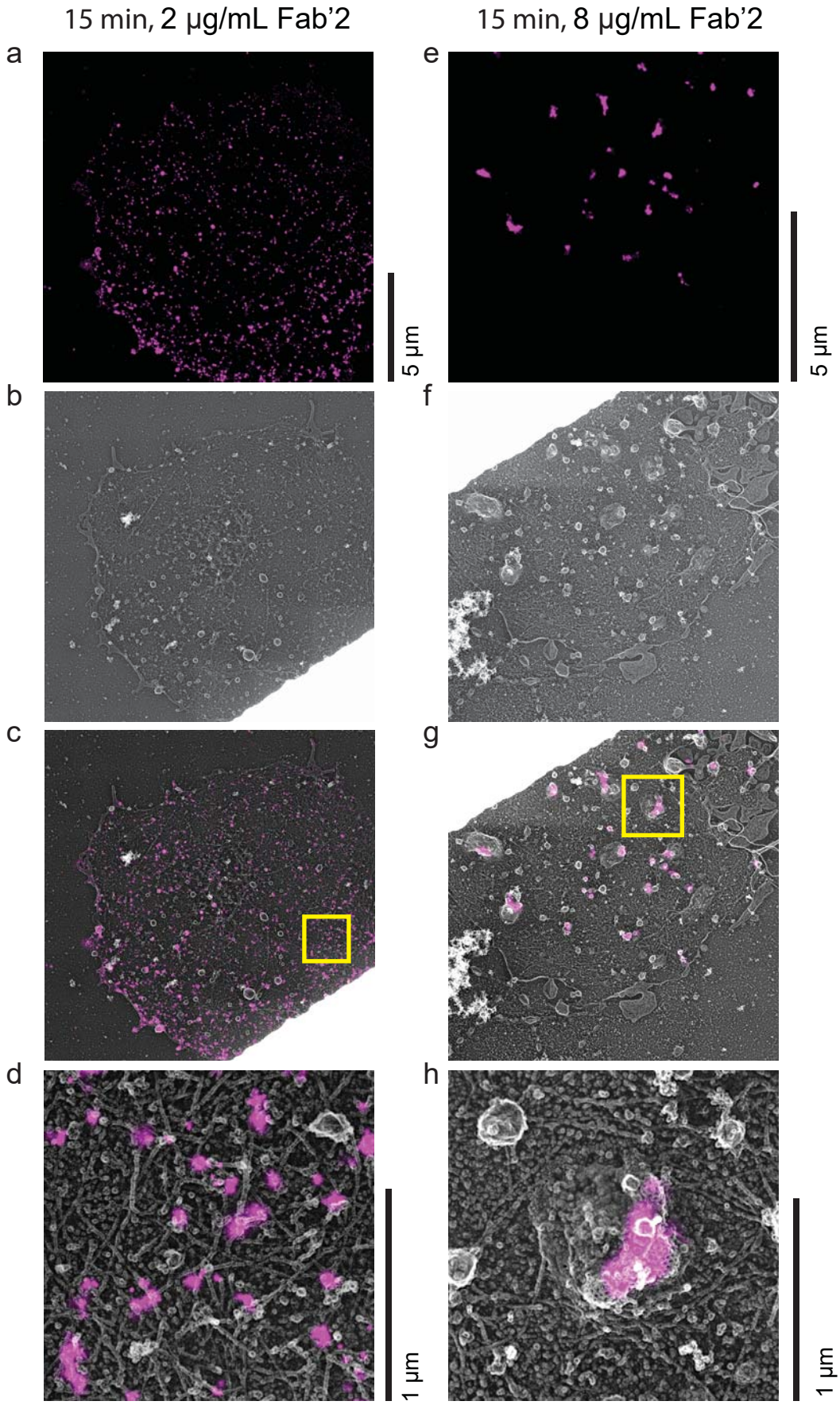

Figure 6

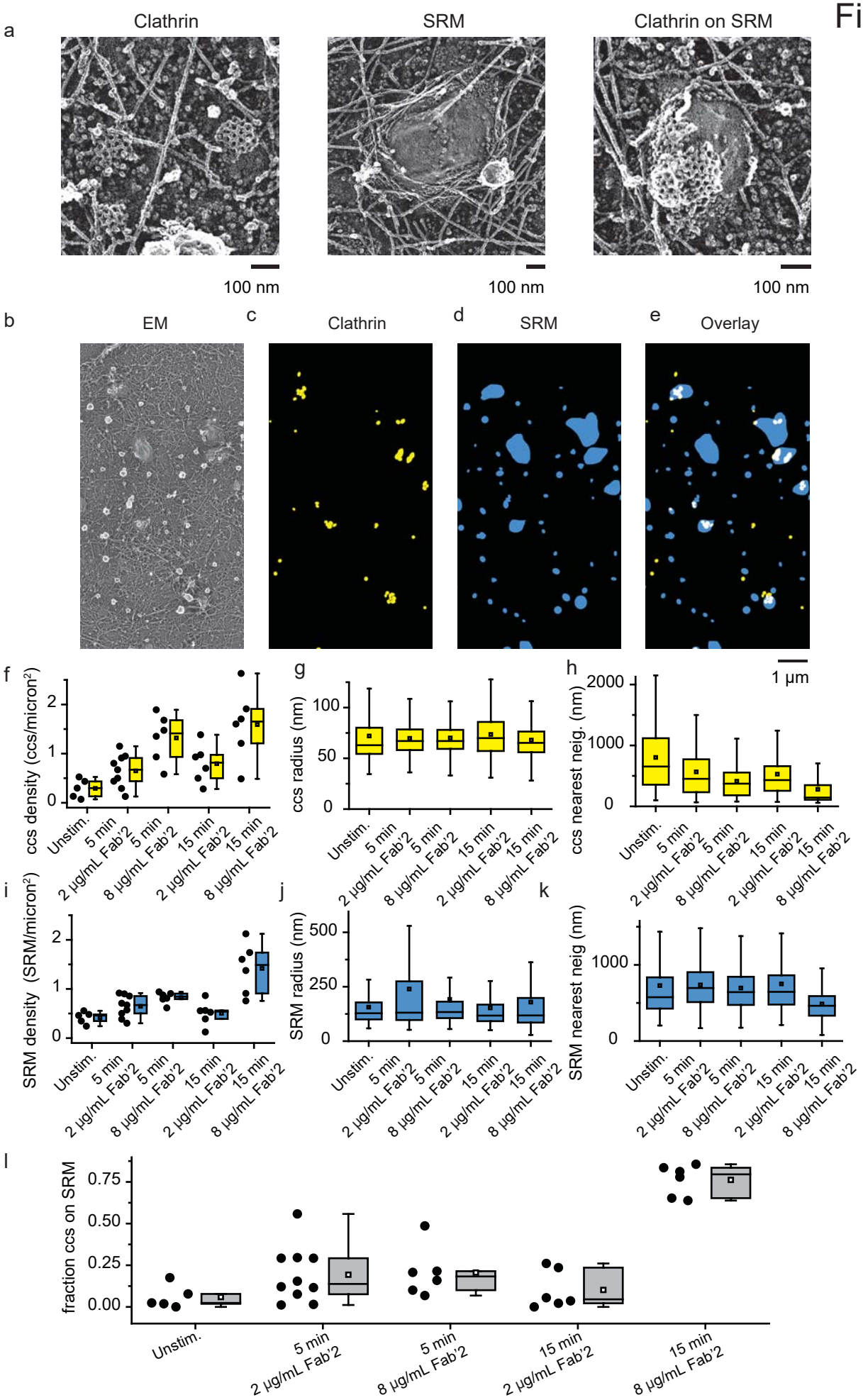
a
Clathrin
SRM
Clathrin on SRM
100 nm
100 nm
100 nm
b
EM
c
Clathrin
d
SRM
e
Overlay
1 µm
f
ccs density (ccs/micron²)
g
ccs radius (nm)
h
ccs nearest neig. (nm)
i
SRM density (SRM/micron²)
j
SRM radius (nm)
k
SRM nearest neig (nm)
Unstim.
5 min 2 µg/mL Fab'2
5 min 8 µg/mL Fab'2
15 min 2 µg/mL Fab'2
15 min 8 µg/mL Fab'2
l
fraction ccs on SRM

Figure 7

a

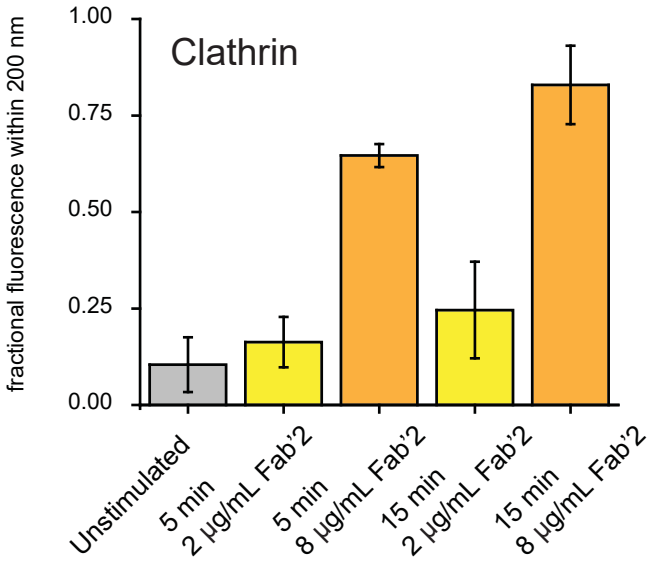
Clathrin
fractional fluorescence within 200 nm
1.00
0.75
0.50
0.25
0.00
Unstimulated
5 min 2 µg/mL Fab'2
5 min 8 µg/mL Fab'2
15 min 2 µg/mL Fab'2
15 min 8 µg/mL Fab'2

b

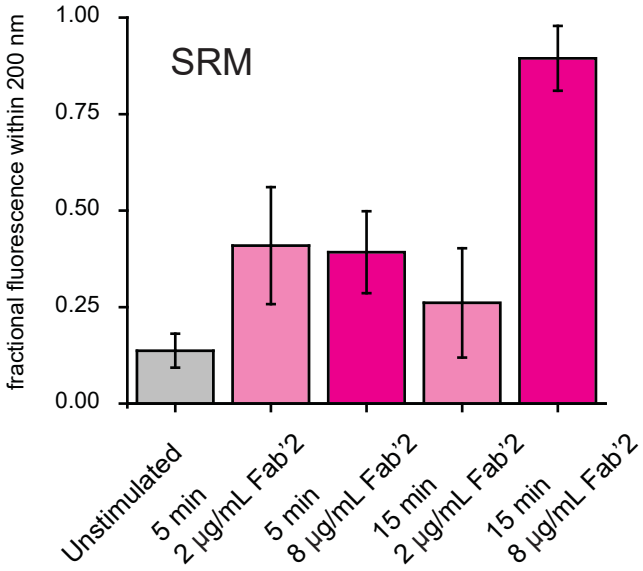
SRM
fractional fluorescence within 200 nm
1.00
0.75
0.50
0.25
0.00
Unstimulated
5 min 2 µg/mL Fab'2
5 min 8 µg/mL Fab'2
15 min 2 µg/mL Fab'2
15 min 8 µg/mL Fab'2

c

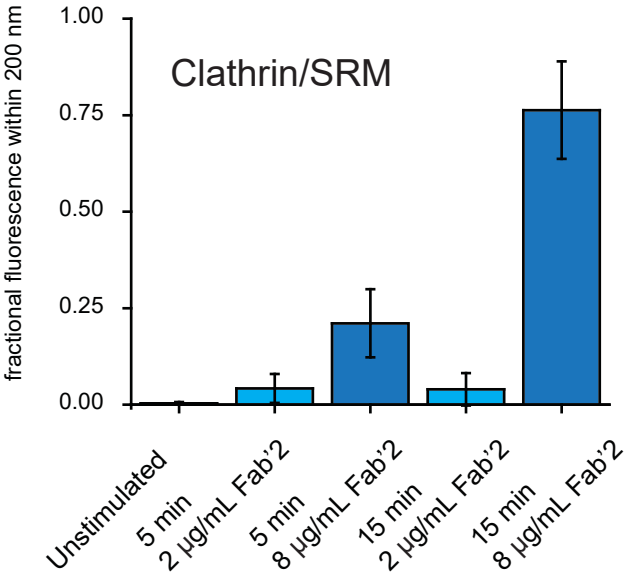
Clathrin/SRM
fractional fluorescence within 200 nm
1.00
0.75
0.50
0.25
0.00
Unstimulated
5 min 2 µg/mL Fab'2
5 min 8 µg/mL Fab'2
15 min 2 µg/mL Fab'2
15 min 8 µg/mL Fab'2

Figure 8

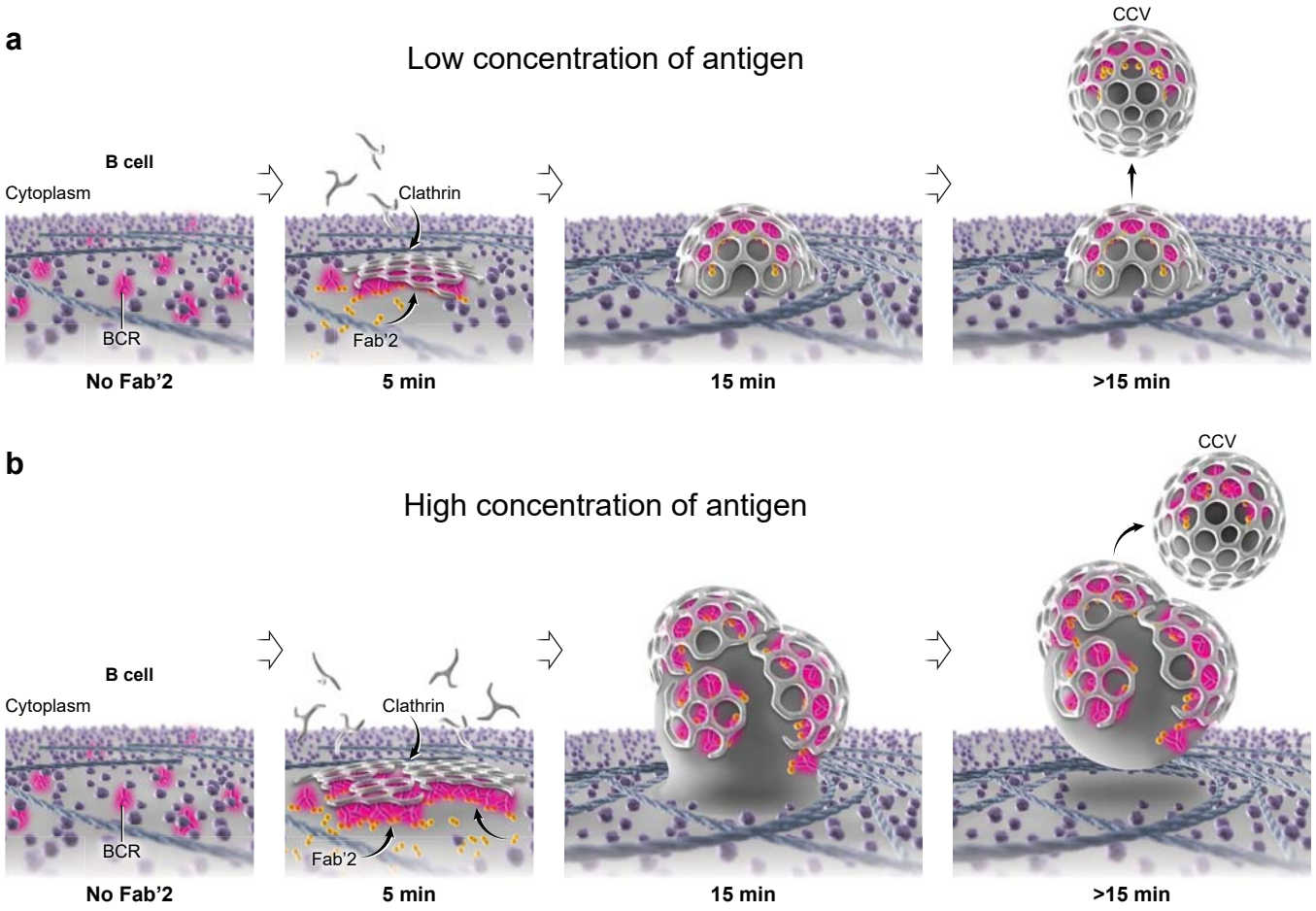
a
Low concentration of antigen
CCV
B cell
Cytoplasm
Clathrin
BCR
Fab'2
No Fab'2
5 min
15 min
>15 min
b
High concentration of antigen
CCV
B cell
Cytoplasm
Clathrin
BCR
Fab'2
No Fab'2
5 min
15 min
>15 min

Supplemental Figure 1

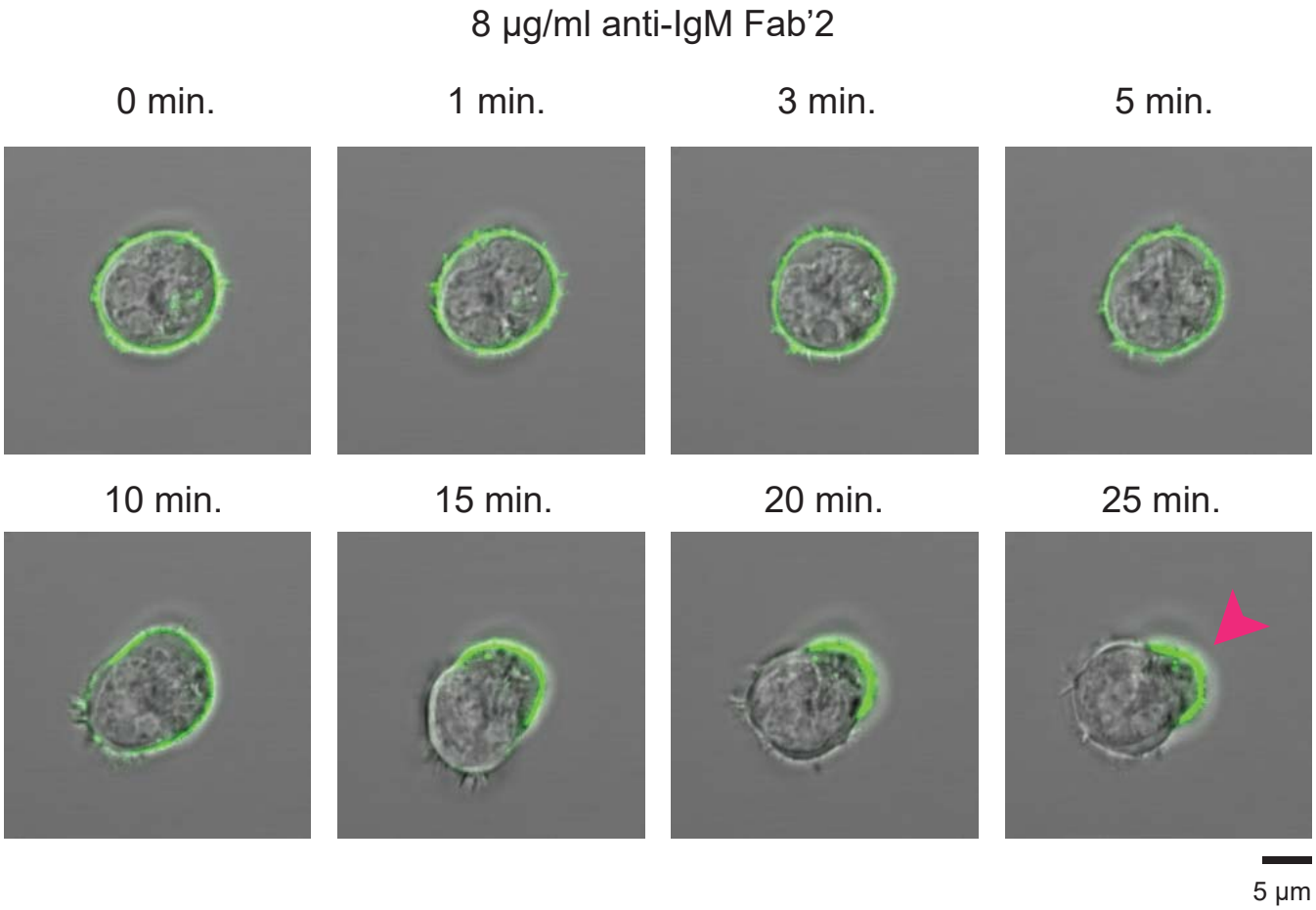

Supplemental Figure 2

Unstimulated

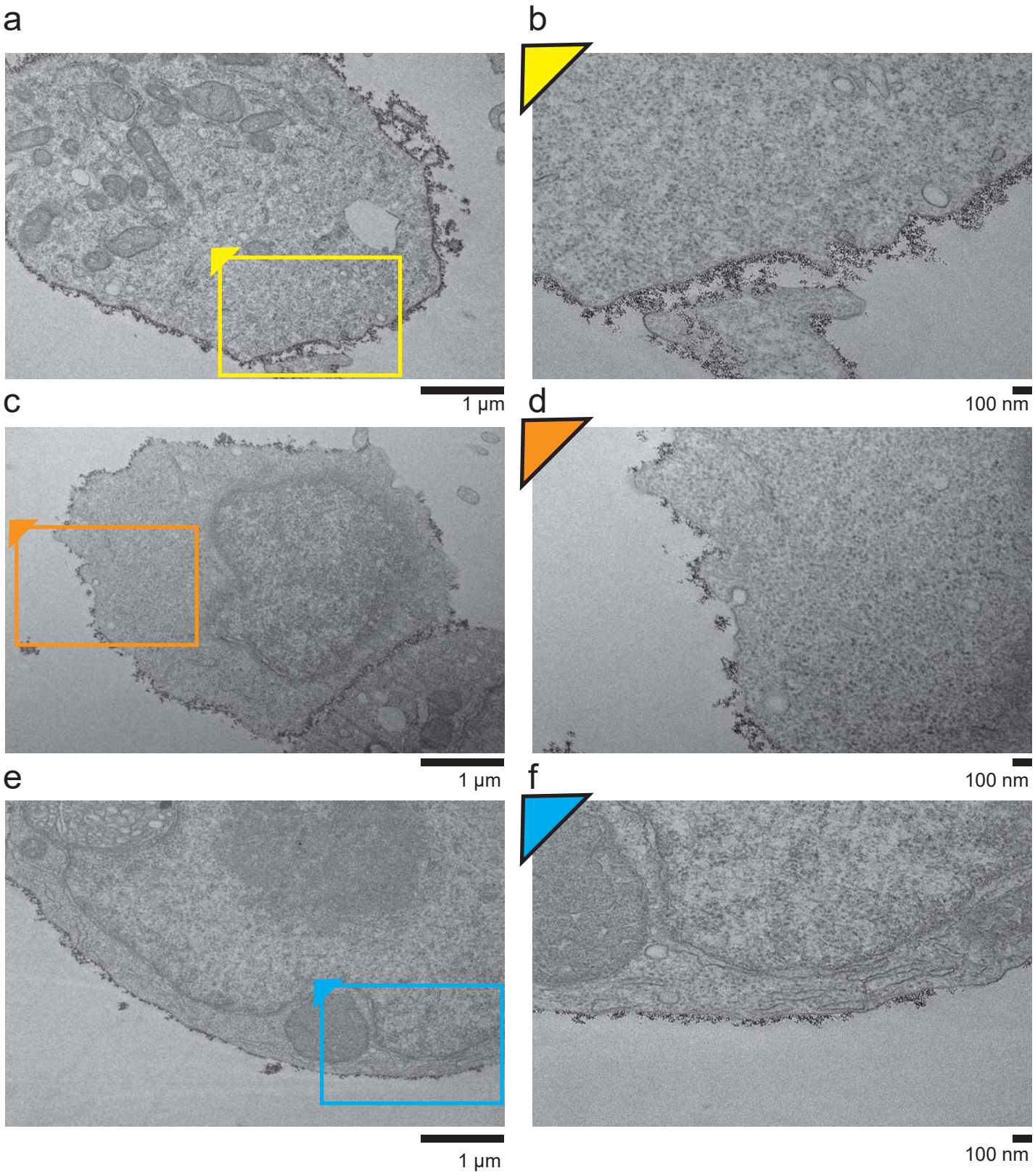

Supplemental Figure 3
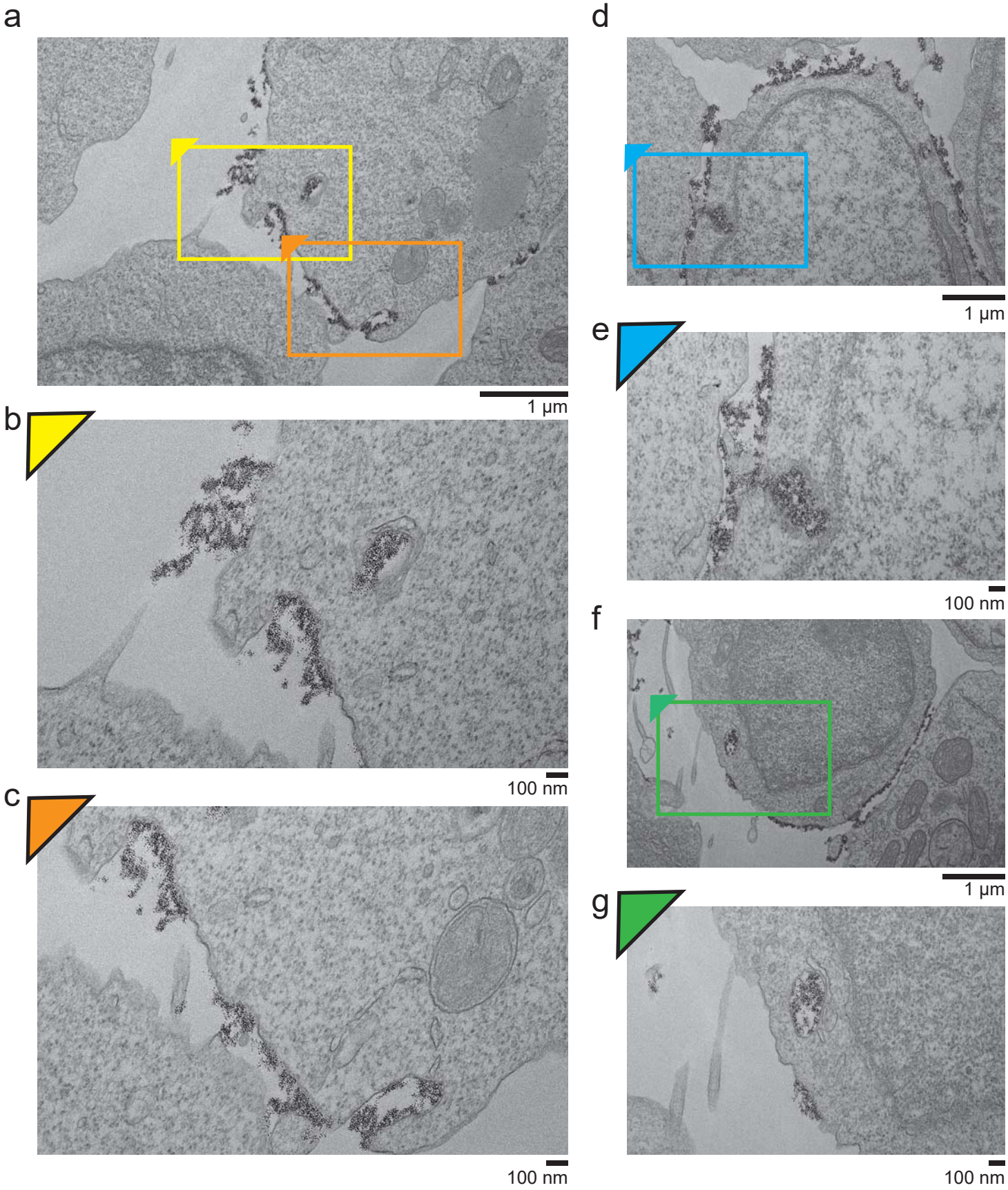
15 min, 8 µg/ml Fab'2